PRESSURE TRANSIENT ANALYSIS AND PRODUCTION ANALYSIS FOR

NEW ALBANY SHALE GAS WELLS

A Thesis

by

BO SONG

Submitted to the Office of Graduate Studies of
Texas A&M University
in partial fulfillment of the requirements for the degree of

MASTER OF SCIENCE

August 2010

Major Subject: Petroleum Engineering

Pressure Transient Analysis and Production Analysis for New Albany Shale Gas Wells

PRESSURE TRANSIENT ANALYSIS AND PRODUCTION ANALYSIS FOR

NEW ALBANY SHALE GAS WELLS

A Thesis

by

BO SONG

Submitted to the Office of Graduate Studies of
Texas A&M University
in partial fulfillment of the requirements for the degree of

MASTER OF SCIENCE

Approved by:

Chair of Committee,   Christine Ehlig-Economides
Committee Members,   Peter Valko
                                  Yuefeng Sun
Head of Department,   Stephen A. Holditch

August 2010

Major Subject: Petroleum Engineering

ABSTRACT

Pressure Transient Analysis and Production Analysis for New Albany Shale Gas Wells.

(August 2010)

Bo Song, B.A., China University of Geosciences (Beijing)

Chair of Advisory Committee: Dr. Christine Ehlig-Economides

Shale gas has become increasingly important to United States energy supply. During recent decades, the mechanisms of shale gas storage and transport were gradually recognized. Gas desorption was also realized and quantitatively described. Models and approaches special for estimating rate decline and recovery of shale gas wells were developed. As the strategy of the horizontal well with multiple transverse fractures (MTFHW) was discovered and its significance to economic shale gas production was understood, rate decline and pressure transient analysis models for this type of well were developed to reveal the well behavior.

In this thesis, we considered a "Triple-porosity/Dual-permeability" model and performed sensitivity studies to understand long term pressure drawdown behavior of MTFHWs. A key observation from this study is that the early linear flow regime before interfracture interference gives a relationship between summed fracture half-length and permeability, from which we can estimate either when the other is known. We studied the impact of gas desorption on the time when the pressure perturbation caused by production from adjacent transference fractures (fracture interference time) and

programmed an empirical method to calculate a time shift that can be used to qualify the gas desorption impact on long term production behavior.

We focused on the field case Well A in New Albany Shale. We estimated the EUR for 33 wells, including Well A, using an existing analysis approach. We applied a unified BU-RNP method to process the one-year production/pressure transient data and performed PTA to the resulting virtual constant-rate pressure drawdown. Production analysis was performed meanwhile. Diagnosis plots for PTA and RNP analysis revealed that only the early linear flow regime was visible in the data, and permeability was estimated both from a model match and from the relationship between fracture half-length and permeability. Considering gas desorption, the fracture interference will occur only after several centuries. Based on this result, we recommend a well design strategy to increase the gas recovery factor by decreasing the facture spacing. The higher EUR of Well A compared to the vertical wells encourages drilling more MTFHWs in New Albany Shale.

DEDICATION

To my parents and my wife

ACKNOWLEDGEMENTS

NOMENCLATURE

a	=	Fraction coefficient, dimensionless
A	=	Drainage Area, ft^2
b	=	Fraction coefficient, dimensionless
B	=	Fluid formation volume factor, rcf/scf
BU	=	Build up
c_t	=	Total compressibility, psi^{-1}
c_t^*	=	Total compressibility, evaluated at average reservoir pressure, psi^{-1}
c_1	=	Slope correlation coefficient, cc/g
c_2	=	Slope correlation coefficient, cc/g
c_3	=	Slope correlation coefficient, cc/g
c_4	=	Slope correlation coefficient, cc/g
EUR	=	Estimated ultimate recovery, Mscf
G_i	=	Original (contacted) gas in place, MMscf
h	=	Payzone thickness, ft
I_{ads}	=	Adsorption Index, hour/hour
k	=	Formation permeability, md
k_f	=	Fracture permeability, md
k_m	=	Matrix permeability, md
k_r	=	Formation permeability in plane, md
k_z	=	Vertical formation permeability, md

L	=	Horizontal well length, ft
m	=	The slope of a graph of pressure versus log Δt, psi/cycle
m_{lf}	=	Slope of a graph of pressure versus square root of elapsed time, psi/$t^{0.5}$
$m(p)$	=	Real gas pseudopressure, psi^2/cp
$MTFHW$	=	Multiple transverse fracture horizontal well
n	=	Valko new decline model parameter, dimensionless
n_f	=	Number of fractures
p	=	Pressure, psia
p_i	=	Initial reservoir pressure, psia
p_L	=	Langmuir pressure, psia
p_{wf}	=	Flowing bottomhole pressure, psia
PDA	=	Production data analysis
PTA	=	Pressure transient analysis
q_g	=	Gas production (surface) rate, Mscf/d
q_i	=	Initial production rate, Mscf/d
Q	=	Cumulative production, Mscf
r	=	Wellbore radius, ft
RF	=	Recovery factor, fraction
RNP	=	Rate normalized pressure, psi
RNP'	=	RNP derivative with respect to logarithm of material balance time
rp	=	Recovery potential
s	=	Skin factor, dimensionless

slope	=	The slope of the linear function of time shift versus adsorption density
SRV	=	Stimulated reservoir volume
S_{ex}^{surf}	=	The total area of exposed surface to matrix particles;
S_w	=	Water saturation, fraction
$S_{\phi f}$	=	The area of surface of fracture space exposed to matrix particles, ft^2;
$S_{\phi m}$	=	The area of surface of matrix pore space exposed to matrix particles, ft^2;
t	=	Elapse time, hours
t_a^*	=	Pseudotime, accounting for desorption, days
t_{ca}^*	=	Material balance pseudotime, accounting for desorption, days
t_e	=	Material balance time, hours
t_p	=	Production time, hours
T_r	=	Reservoir temperature, ºF
t_{sup}	=	Superposition time, dimensionless
V_{ads}	=	Gas volume can be adsorbed by a rock of unit mass, scf/g
V_{des}	=	Gas volume desorbed by a rock of unit mass, scf/g
V_L	=	Langmuir volume, the maximum gas volume can be adsorbed, scf
V_{ph}	=	The adsorbed gas volume at the higher pressure, scf
V_{pl}	=	The adsorbed gas volume at the lower pressure, scf
$V_{\phi f}$	=	Fracture space saturated by gas, scf
$V_{\phi m}$	=	The pore space volume in matrix saturated by gas, scf
w	=	Fracture width, ft
x_f	=	Hydraulic fracture half length, ft

Z^* = Gas derivation factor adjusted to account for desorption, dimensionless

z_w = Horizontal well vertical position, ft

Dimensionless variables

EUR_D = Dimensionless estimated ultimate recovery

q_D = Dimensionless production rate expression

Q_D = Dimensionless cumulative production

Greek variables

α = Shape factor depending the size and geometry of matrix, dimensionless

λ = Interporosity flow coefficient, fraction

θ = Coverage fraction of the surface, dimensionless

μ = Viscosity, cp

μ_g = Gas viscosity, cp

ρ_{ads} = Adsorption density, g/cc

ρ_{ads}^{surf} = Adsorbed gas density, g/cc

ρ_{ra} = Adsorbed gas volume released from unit exposed surface area, scf/ ft^2

ρ_{rock} = Rock density, g/cc

τ = Valko new decline model parameter, dimensionless

ϕ = Porosity, fraction

ω = Storage ratio, fraction

ω_{mod} = Storage ratio accounting for desorption, fraction

Subscripts

a	=	Pseudo
ads	=	Adsorbed
c	=	Material balance
ca	=	Material balance pseudo
D	=	Dimensionless variables
des	=	Adsorbed
e	=	Material balance
ex	=	Exposed
f	=	Fracture
g	=	Gas
gas	=	Gas
i	=	Initial
L	=	Langmuir
lf	=	Linear flow
m	=	Matrix
mod	=	Modified
p	=	Production
ph	=	Higher pressure state
pl	=	Lower pressure state
r	=	Reservoir
ra	=	Release to surface area

rock	=	Reservoir
sup	=	Superposition
w	=	Water
wf	=	Sandface
z	=	Vertical direction
ϕf	=	Porous space of natural fracture system in shale gas reservoirs
ϕm	=	Porous space of matrix pore system in shale gas reservoirs

Superscripts

surf	=	Surface
‾	=	Average property
*	=	Altered variables

TABLE OF CONTENTS

LIST OF FIGURES

LIST OF TABLES

CHAPTER I

INTRODUCTION: BACKGROUND AND LITERATURE REVIEW

Chapter I is aimed to give a brief introduction of shale gas resources in United States as well as a particular gas shale play, the New Albany Shale, as a background. Besides, the literature review including several aspects, such as gas storage and transport mechanism of shale gas, pressure transient behavior of shale gas wells and production analysis of shale gas wells, are summed to provide guidance for the research in this thesis.

1.1 Shale Gas Resources in United States

Unconventional natural gas resources, which include shale gas, tight gas sands, coalbed methane and deep basin-centered gas system, play a significant role in today's gas supply in U.S and are an important source for gas production and gas reserve growth in the future. Gas shales, the formations which are considered as both source rocks and reservoirs, are supposed to contribute a lot to the future gas production. Traditionally shale formations were only thought as source rocks or cap rocks, but not reservoir rocks where hydrocarbons accumulate. However, the success of Barnett Shale has proved that gas can be produced from shale reservoirs economically and this revolutionary success led developments of many other shale gas reservoirs (Arthur, Bohm and Layne, 2008).

_____

This thesis follows the style of *Society of Petroleum Engineers (SPE)*.

By 2008, the natural gas resource potential for gas shale in USA was estimated to be 500-1000 Tcf. Many shale gas plays have been found (Figure 1) in the contiguous United States (Cipolla *et al* 2009). Deregulation of natural gas prices, improvement of stimulation techniques and horizontal drilling made the economic development of shale gas reservoirs possible (Arthur, Bohm and Layne, 2008).

Typically, the shale gas reservoirs exhibit a net thickness varying from 50 ft to 600 ft. Porosity varies from 2% to 8% and total organic carbon (TOC) ranges from 1% to 14 %. The depth of shale gas reservoirs also varies apparently. A shallow depth can be 1000 ft while a deep one can be up to 13000 ft (Cipolla *et al* 2009). Gas is stored as free gas in the limited pore space of the rocks, such as micro-pores and natural micro-fractures, and a sizable fraction of the gas in place is stored as adsorbed gas which is adsorbed on the surface of matrix particles (Lane, Waston and Lancaster, 1989).

Figure 1. Gas Shale Plays in Lowe 48 United States

Unlike conventional natural gas resources, shale gas is more difficult to be produced due to extremely low effective permeability. Typically, shale permeability ranges from 10 to 100 nano-Darcy (10^{-5}-10^{-4} md) (Cipolla *et al* 2009). Though natural micro-fractures often occur in the shale formation, hydraulic fracture stimulation is still necessary to induce flow in most cases and today the strategy is to create a fracture network so that a huge reservoir surface can be effectively connected to the wellbore. However, unlike conventional hydraulic fracture treatments that use high viscosity fluids to reduce fracture complexity and promote planar fractures and allows the placement of high concentrations of large proppant, stimulation treatment in shale gas reservoirs may use low viscosity fluid to promote fracture complexity. The fracture treatment approach is totally different from conventional fracture treatment (Cipolla *et al* 2009).

In shale gas reservoirs, it is very common that water is produced with gas. Today, surface facilities designed to handle water production enable much better gas production rates (Kalantari Dahaghi and Mohaghegh, 2009)

Shale gas reservoirs are typically comprised of two distinct porous media: the shale matrix containing the majority of gas storage in the formation but with a very low permeability and the fracture network with a higher permeability but low storage capacity. It is believed that in most cases shale gas is stored as "free gas" in both shale matrix and natural fracture system and as "adsorbed gas" on the surface of matrix particles. Since adsorption is considered as an unconventional mode of gas storage, its effect was usually ignored in conventional reservoir engineering analyses. However, even back to 1980's, practical reports indicated that adsorbed gas might account for up

to over 80% of gas storage in some shale gas plays. Moreover, recent work indicates that gas desorption affects the production behavior and pressure transient behavior of gas wells significantly, particularly in the stimulated wells. Therefore, gas adsorption, which might and should be a very important gas storage mechanism, has been taken into account for modeling shale gas reservoir as shale gas exploration develops (Lane, Waston and Lancaster 1989).

The use of horizontal well drilling and multistage hydraulic fracturing appear to be key aspects for successful development of the shale gas resource. The horizontal well technology was adapted for shale gas development to provide increased wellbore exposure to the reservoir area while hydraulic fracturing, the other technology key for facilitating economical recovery of natural gas shale, is used to provide significantly more contact with reservoir which is needed because the permeability is very low. The combination of the two key aspect results in the typical well type applied in shale gas development, the multistage transverse fracture horizontal well, in which multi hydraulic fractures are produced normal to the horizontal well trajectory (Figure 2).

From a historic perspective, the shale gas development including the success of Barnett Shale has demonstrated the economic potential of shale gas through the use of horizontal well completions and hydraulic fracturing techniques. Barnett horizontal wells have laterals ranging from 1,500 to more than 5,000 feet and for these wells to be economically productive, they require hydraulic fracturing. Besides that, the development of the Marcesllus Shale has been made possible also based on the two technological advances. Although current development practices in the Marcellus shale

involve the drilling of both horizontal and vertical wells, hydraulic fractured horizontal wells are expected to become predominant for the play (Arthur, Bohm and Layne, 2008). It is reasonable to believe that horizontal well completions combined with hydraulic fracturing will provide the best opportunity for producing economic volumes of natural gas from shale gas plays.
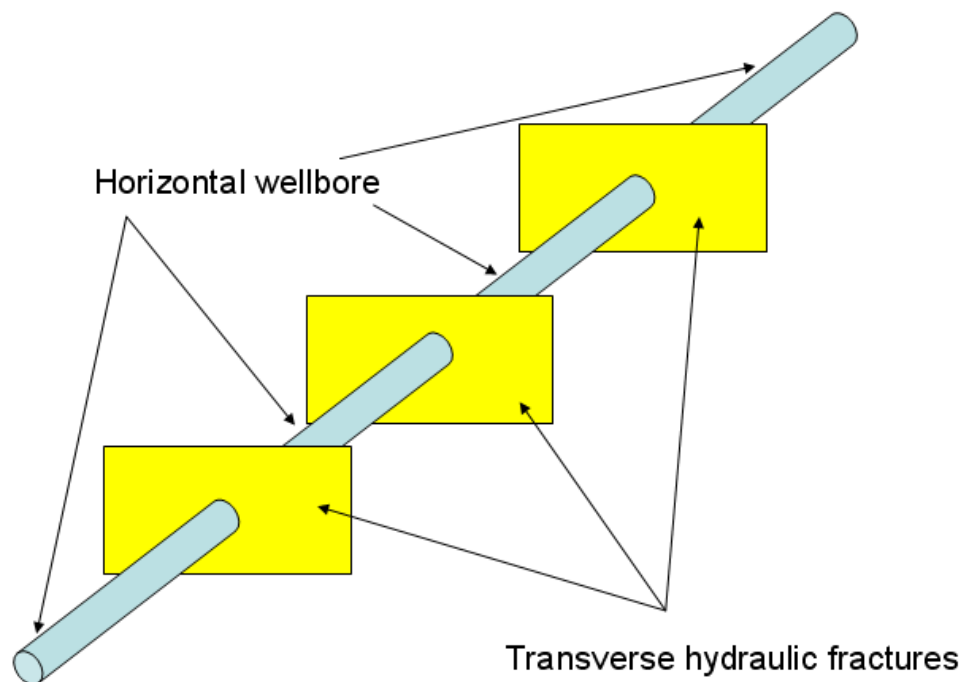
Figure 2. Illustration of Multistage Hydraulic Fracture Horizontal Well

1.2 Introduction of New Albany Shale Gas Play

The New Albany Shale is predominantly an organic-rich brownish-black and grayish-black shale, and is located over a large area in southern Indiana and Illinois and in Northern Kentucky (Figure 3). The shale is present in the subsurface throughout the

Illinois Basin (Zuber *et al* 2002). The total gas content of New Albany Shale has been estimated to be 86 TCF (Kalantari Dahaghi and Mohaghegh 2009). The depth of shale appears at 500 ft to 2000 ft on average. The gross thickness of the organic shale varies form 100 ft to 150 ft, and is generally separated into 4 main stratigraphic intervals from top to bottom (Figure 4): Clegg Creek, Camp Run/Morgan Trail, Selmier and Blocher (Zuber *et al* 2002). Natural fractures occur in the shale formation and are believed to provide the effective permeability in these zones. The density of natural fractures is not very high, but this doesn't preclude the economic gas potential in New Albany Shale play (Dahaghi and Mohaghegh 2009).

New Albany Shale has been considered as a productive gas reservoir for many years. Over 200 wells had been drilled by the mid 1990s. Generally, gas production in New Albany Shale ranges from 30 to 100 Mscf/D and water production is very variable. Some wells made very little water while others made even more than 1000 B/D (Zuber *et al* 2002).
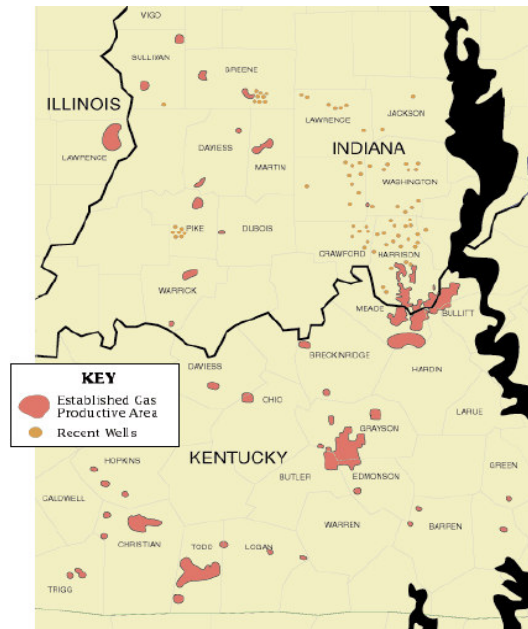
Figure 3. Productive Area of New Albany Shale
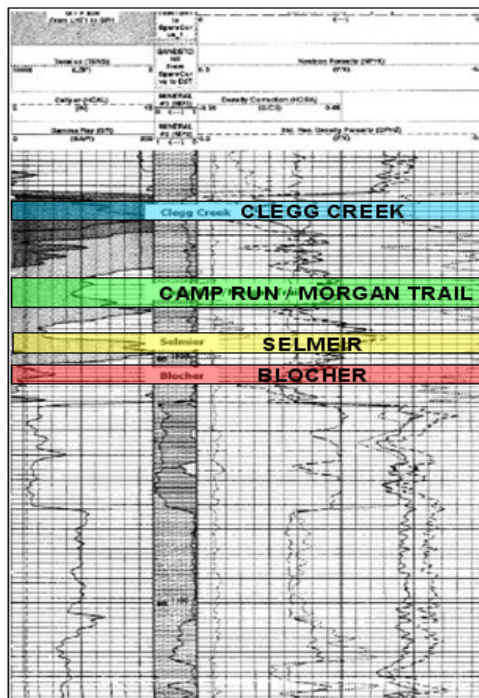
Figure 4. Stratigraphy of New Albany Shale

1.3 Literature Review

During the last tens of years, the industry has realized that the important role of gas adsorption, which makes shale gas and other unconventional gas resources such as coalbed methane different from the conventional gas resources. The storage and production mechanisms of gas in shale become a significant issue for both reserve estimation and production so that an appropriate conceptual model for shale gas reservoir is very necessary. Lane, Waston and Lancaster (1989) indicated that in shale reservoirs, gas is stored both as free gas in matrix pores and fractures and as adsorbed gas on the surface of matrix particles. Kuuskraa *et al* (1985) also indicated the importance of gas adsorption to gas recovery and behavior of shale gas wells through the investigation of Shale Gas in Ohio, West Virginia, and Kentucky. Zuber *et al* (2002) provided a conception model illustration in their paper for a comprehensive evaluation for New Albany Shale. "Triple porosity/Dual permeability Model", which is a more detailed conceptual model including the consideration of both free gas and adsorbed gas was given by Schepers *et al* (2009). Besides those articles about gas shales, Rushing, Perogo and Blasingame (2008) provided a conceptual model for coalbed methane, which is considered to partially or totally share the same mechanism of gas storage and production with gas shales. For gas adsorption/desorption, the very important element in shale gas resources, Schepers *et al* (2009) and Lane, Lancaster and Waston (1990) indicated that Langmuir Model provides the best description. Moreover, it is also the most popular model for gas adsorption/desorption.

With the development of technology of horizontal well and hydraulic fracturing, economic production from gas shale is achieved. Though there is longitudinal and transverse fracturing for horizontal wells, almost all the recently reported fracturing application in the industry is the later option (Wei and Economides 2005) and multistage fractured horizontal wells are widely in use in shale gas development, such in the plays of Barnett Shale and Marcellus Shale (Arthur, Bohm and Layne, 2008). Therefore, understanding the behavior multi-transverse-fractured horizontal well (MTFHW) is important to understand the well performance. The Flow regime issue of MTFHW was discussed several researchers: Clarkson *et al* (2009), Freeman *et al* (2009) and Al-Kobashi *et al* (2006) offered flow regimes analyses of MTFHW and a common conclusion emerges from their work: potential reservoir flow regimes appear in the sequence of linear flow normal to fracture face, then interference between fractures, then compound linear flow (linear flow normal to horizontal well axis), then pseudoradial flow around the MTFHW system (if possible), and then boundary flow (Not likely, but if present could be due to interference with adjacent similar well).

Production analysis for shale gas wells is challenging. Ilk *et al* (2008) used to develop an empirical formulation, the "Power-Law Exponential" rate decline model to perform production analysis and estimate gas-in-place/reserves for unconventional gas reservoirs. Valko (2009) developed a new decline curve model, which is both empirical and mechanical but not analytical to estimate the estimated ultimate recovery for individual well via calculating recovery potential. This approach is based on the analyses of over 7,000 gas wells in Barnett Shale and it is more direct than the former one.

The above introduction provides a general understanding of shale gas, the significant resource in today's American oil and natural gas industry. New Albany Shale is also briefly described because it is the target case on which the research work in this thesis focuses. The literature review referring to conceptual model issue, PTA issue and PA issue establishes a basis based on which the further research can be performed. The following chapters will focus on an appropriate conceptual model for the shale gas reservoir (Chapter II), rate decline analysis for New Albany Shale Gag Wells (Chapter III), drawdown pressure transient behavior in Multi-transverse fractured horizontal wells (MTFHWs) (Chapter IV) and the particular field case study of New Albany Shale (Chapter V), and all the further research work described in the following chapters benefits from the previous achievements.

CHAPTER II

CONCEPTUAL MODEL FOR SHALE GAS

Before a play is developed, it is essential to understand how mechanisms of fluid storage and transport in the reservoir affects reserves, well behavior, production performance, and even the ultimate recovery. An appropriate conceptual model can help estimate reserves and the recovery factor more accurately and forecast the well behavior and performance. Chapter II is aimed to describe the "Triple porosity/Dual permeability" model, and how it explains gas storage and transport mechanisms in shale formations.

2.1 Gas Storage Mechanism

Gas in shales is stored in two ways: free gas and adsorbed gas. The former is stored both in micro-pore space in the matrix and natural fractures in shales, and the later is stored on the surface of shale matrix particle by adsorption.

Free gas is a relative conception compared with adsorbed gas. It is essentially like the gas in conventional gas reservoirs in which pore space (or with fractures) provides the storage space. In shale gas reservoirs, natural fractures and micro-pores inside the matrix provide the storage for free gas. Therefore free gas is stored in a dual-porosity system which is like what we use for describing conventional natural fracture reservoirs. Matrix pores provide a relatively higher storage capacity than natural fractures due to their astronomically large amount though individual pore is very small and lower permeability than natural fractures due to their extremely small dimension and more complex connection.

Adsorbed gas, which might account for a big part of gas storage in gas shales, is stored by a different physical mechanism. Adsorption is the mechanism which makes this gas bound on the surface of matrix particles. A "Triple porosity" Model is appropriate to describe the gas storage mechanism (Figure 5) because it includes both the free gas and adsorbed gas. Briefly speaking, triple porosity is dual porosity system combined with gas adsorption. The reason for "Triple" is that free gas is stored in dual porosity system comprised of the matrix micro-pores (the first porosity) and natural fractures (the second porosity) and gas adsorption is considered as the third porosity though in reality the storage space is not pores or fractures but the particle surface. More will be said about gas adsorption and desorption in Section 2.3.
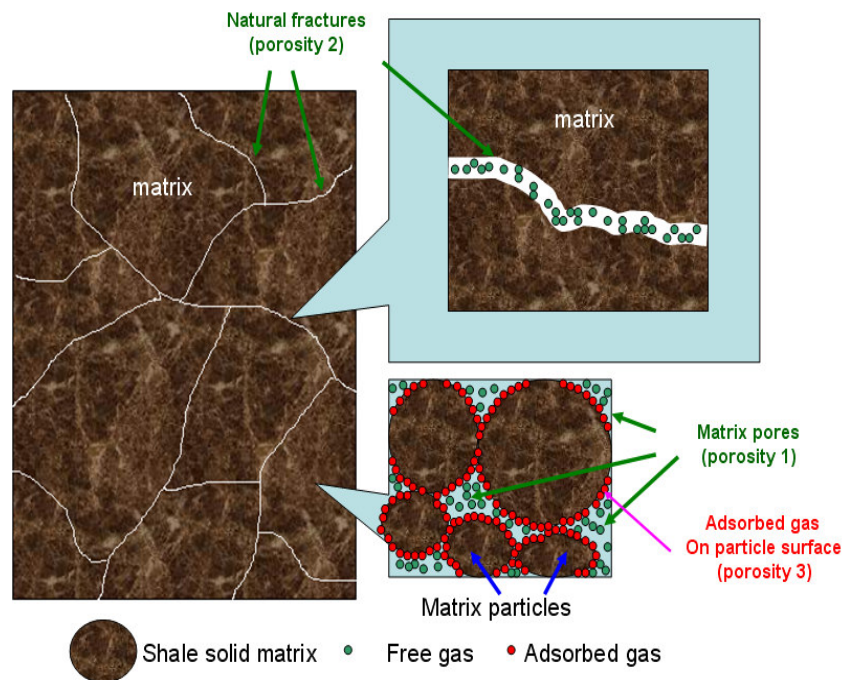
Figure 5. Triple Porosity Storage Model in Gas Shales

2.2 Gas Transport Mechanism

Schepers *et al* (2009) used to provide a conceptual model for gas shales. Apart from the similar storage consideration (dual porosity combined with gas adsorption) to other researchers, this model claims some different views of the gas flow mechanism. Figure 6 illustrates the model provided by Schepers *et al*. According to the lower part of Figure 6, two points should be highlighted: First, Schepers *et al* didn't indicate the adsorption gas will diffuse into fracture system as well when it diffuses into matrix pore system; Second, the fluid flow within matrix micro-pore system and the flow from matrix micro-pore system to fracture system is following Darcy-Flow rule which means the transport mechanism is the flow in porous media due to pressure gradient.
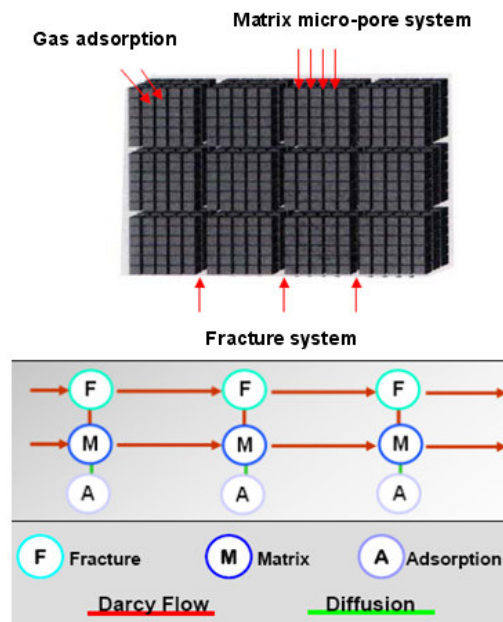
Figure 6. Conceptual Model for Gas Shales (Modified from Schepers *et al* 2009)

The "Triple porosity/Dual permeability Model" given by Schepers *et al* is an appropriate description for gas shales. However, due to the two emphasized points mentioned above, some considerations aren't included in this model. A modified "Triple porosity/Dual permeability Mode" is provided in this thesis based on the Schepers' great contribution to the conceptual description for gas shales. Considering the first highlighted point, it appears that adsorbed gas will also be released into the fracture system as well as into matrix pore system. Matrix solid particle surface is not only exposed to the matrix pores, but also exposed to fracture space. Though compared to the area of matrix particle surface exposed to matrix pores, that area of particles surface exposed to fractures is much smaller, its existence should not be ignored since the fact is factures are the space surrounded by the matrix. The second point is essentially about transport mechanism inside matrix pore system and from matrix to fractures. Schepers' model indicates definitely it is a porous medium flow that controls the gas transport. Zuber *et al* (2002) also indicated the same view in their paper about New Albany Shale (Figure 7).
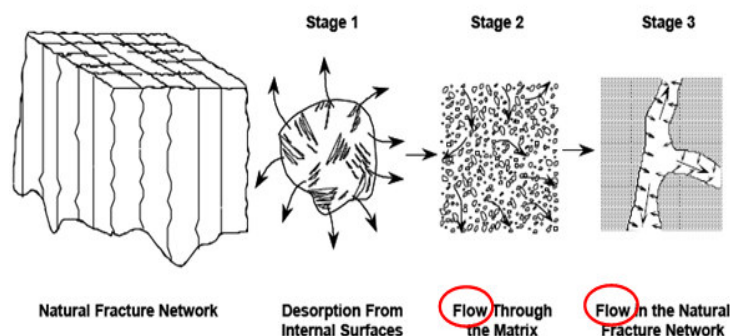
Figure 7. Conceptual Model for Gas storage and Transport (Zuber *et al* 2008)

Wang and Reed (2009) discussed this more specifically: Two main types of porous media are included in gas shales, pores and fractures. The former can be subdivided into two types as nonorganic pores and organic pores, and the later contains subtypes as natural fractures and hydraulically induced fractures. Pores formed by organic substance (organic pores) inside matrix is believed to act as a porous medium even though more detailed mechanism of gas flow through organic matters is speculative. All above, the matrix micro-system is considered as a porous media according to those researchers though common sense of shale matrix's low permeability may lead people to negate this.

However, not all agree that the matrix pore system acts like a porous medium. Rushing *et al* (2008) indicated in describing their description coalbed methane model that gas transport in matrix pore space is due to diffusion resulting from a concentration gradient (Figure 8) because the permeability is too low to activate Darcy-flow. This indirectly denies the view of porous medium. However, whether this description is also suitable for shale gas is questionable because though coalbed methane shares many aspects in common with gas shales, they are not the same.
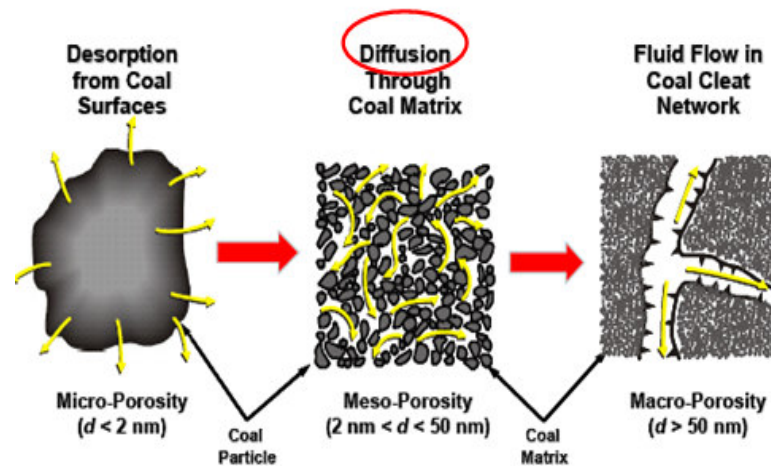
Figure 8. Stage Gas Production Process in Coalbed Methane (Rushing *et al* 2008)

Even the industry contains both the two opinions. In the commercial software "Ecrin" developed by Kappa Engineering, the reservoir model also contains two options, two porosity model and homogeneous-diffusion model for gas shales and coalbed methane. However, it is not possible to model simultaneously diffusivity and double porosity in our current implementation in Ecrin.

This analysis in this thesis assumes that the mechanism of gas flow through matrix pore system is flow in porous medium. There is not sufficient evidence to prove absolutely absence of diffusion through shale matrix and even Schepers himself stated the release and transport mechanisms are characterized by desorption, diffusion and Darcy-flow (though the diffusion is likely to occur in individual matrix pore after desorption according to Figure 6). However, flow in the porous medium is still believed to be the dominate mechanism even if diffusion does exist at the same time. This is not only because of its application in simulation work, as shown by Schepers *et al* (2009) ,

but also because of the research in more microscopic mechanics, as described by Wang and Reed (2009). In general, the concept diffusion through matrix was described based on coalbed methane and not shale gas. The gas transport mechanism through matrix in coalbed methane might be really different from that in gas shales.

To solve the above two highlighted points, a more accurate and integrate mechanism of shale gas transport can be described by flow chart shown as Figure 9.
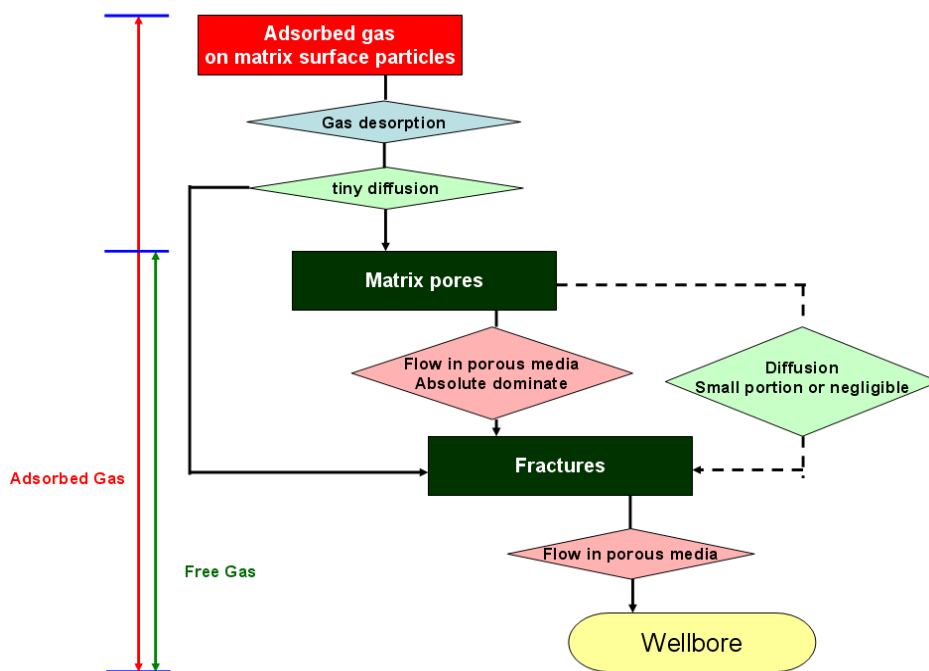
Figure 9. Gas Transport Mechanism in Gas Shales

The transport process can be described in this way: free gas will flow through matrix pores (primary porosity) into the fracture system (secondary porosity) due to pressure gradient, driven by a mechanism of fluid flow in porous media (diffusion might exist but

can be neglected); then free gas will flow to the wellbore through fractures. For adsorbed gas, desorption will occur when pore pressure decreases, and adsorbed gas molecules have the potential to move and diffuse to the pore space from particle surfaces. The duration of the diffusion (diffusion time) happening in such small pores which are usually in micro scale is considered to be negligible. After that, the adsorbed gas essentially becomes free gas and the future transport will follow the same way with the original free gas, and the mechanisms of flowing through matrix pore system and fracture system is also the same.

By now, a more appropriate conceptual model for gas shales has been described. The meaning of "Triple Porosity/Dual Permeability" in gas shales is that matrix pores, fractures and gas adsorption are the three effective porosities for storage while matrix pores and fractures are the two permeable porous media through which gas flows. Understanding the essence of the model is the basis for future research in pressure transient behavior and production performance of shale gas wells. Figure 10 provides a clear illustration.
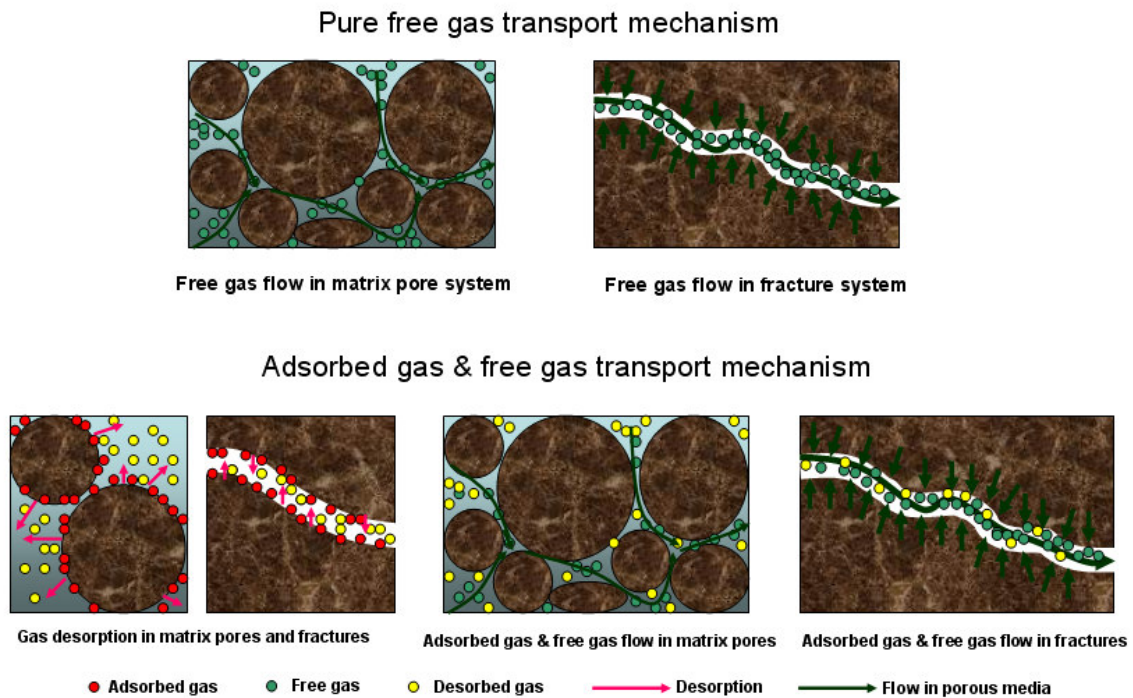
Figure 10. Illustration of Gas Transport Mechanism in Gas Shales

2.3 Gas Adsorption/Desorption Model

Gas adsorption is a surface phenomenon and is predominately a physical bond caused by the inter-molecular attractive forces (i.e., Van der Waals forces) (Rushing *et al* 2008) while desorption is the converse process of adsorption.

The Langmuir Model is the most commonly used models for quantifying the description of gas adsorption/desorption. The mathematic expression of this model is:

$$V_{ads} = \frac{V_L p}{p_L + p} \dots\dots\dots\dots\dots\dots\dots\dots\dots\dots\dots\dots\dots\dots\dots\dots\dots\dots\dots\dots\dots\dots\dots\dots\dots \text{(1)}$$

Where:

V_{ads}, [scf/ton], the gas volume can be adsorbed by a rock of unit mass;

V_L, [scf], Langmuir volume, the maximum gas volume can be adsorbed;

p_L, [psi], Langmuir pressure, at which half of Langmuir volume gas can be adsorbed;

p, [psi], random pressure

This model assumes there is no change in temperature. Actually, temperature will affect the gas adsorption capacity, and specifically, the higher the temperature the less gas can be adsorbed. In the Langmuir formula, temperature is not considered because of an assumption that temperature does not change for the problem under consideration. That is the reason why the plot of the Langmuir formula is called a "Sorption Isotherm". This assumption is reasonable is because reservoir flow processes are assumed to be isothermal. A typical sorption isotherm curve is illustrated as Figure 11.
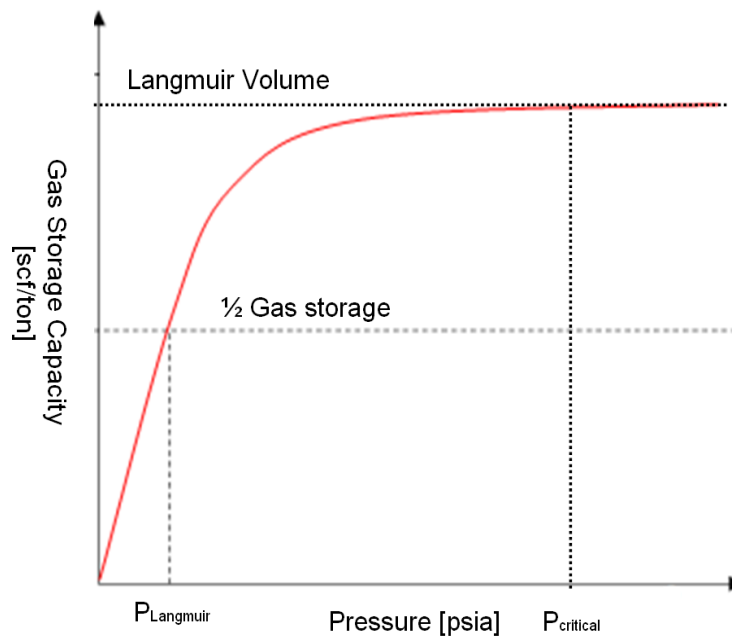
Figure 11. Illustration of Typical Gas Adsorption/Desorption Isotherm

For a fixed temperature, the Langmuir volume and Langmuir pressure control the shape of sorption isotherm. For any pressure, the quantity of adsorbed gas can be calculated. There is only one discrepancy between the mathematic and physical description of the adsorption/desorption process. From a theoretical prospective, as pressure trends to infinity, gas storage capacity is going to be infinitely close to Langmuir volume but it can never reach the Langmuir volume value theoretically. In reality, the adsorbed gas starts to be desorbed when pressure decreases from some high level to a point called the "critical pressure". Below the critical pressure the desorption process will follow the Langmuir model precisely. The small discrepancy doesn't deny the reasonability of Langmuir model because usually, the gas adsorption capacity difference between infinitely high pressure and critical pressure is so small that it can be negligible. Therefore, Langmuir model accounts for the essential gas adsorption/desorption behavior.

Besides the mathematic expression (Eq 1), Langmuir model can be expressed by some equivalent expressions. Another popular expression is as following:

$$\theta = \frac{p}{p_L + p} \quad \dots\dots\dots\dots\dots\dots\dots\dots\dots\dots\dots\dots\dots\dots\dots\dots\dots\dots\dots\dots\dots\dots\dots\dots\dots\dots\dots\dots\dots\dots\dots\dots\dots \quad (2);$$

Where,

p_L, [psi], Langmuir pressure, at which half of Langmuir volume gas can be adsorbed;

p, [psi], random pressure;

θ, [dimensionless], coverage fraction of the surface, essentially V_{ads} / V_L

$\theta \in [0,1]$.

Another issue about gas desorption is desorption time. In some circumstances, as the pressure decrease, adsorbed gas molecules are expected to be desorbed from the matrix particle surface. However, even when the pressure condition allows the occurrence of gas desorption, it might be delayed in time. The time interval between the time when pressure drops to the level for desorption and that when desorption really take place is termed desorption time. However, for convenience, assumption of instantaneous desorption is usually made.

The commercial software Kappa Ecrin uses the Langmuir model to describe the gas desorption in the shale gas model. The parameters controlling gas desorption in the model parameter input dialog window (Figure 12) include Langmuir pressure and adsorption density. As described above, it is Langmuir pressure and Langmuir volume that controls the gas desorption behavior. The later terminology called "adsorption density" could lead to some confusion.
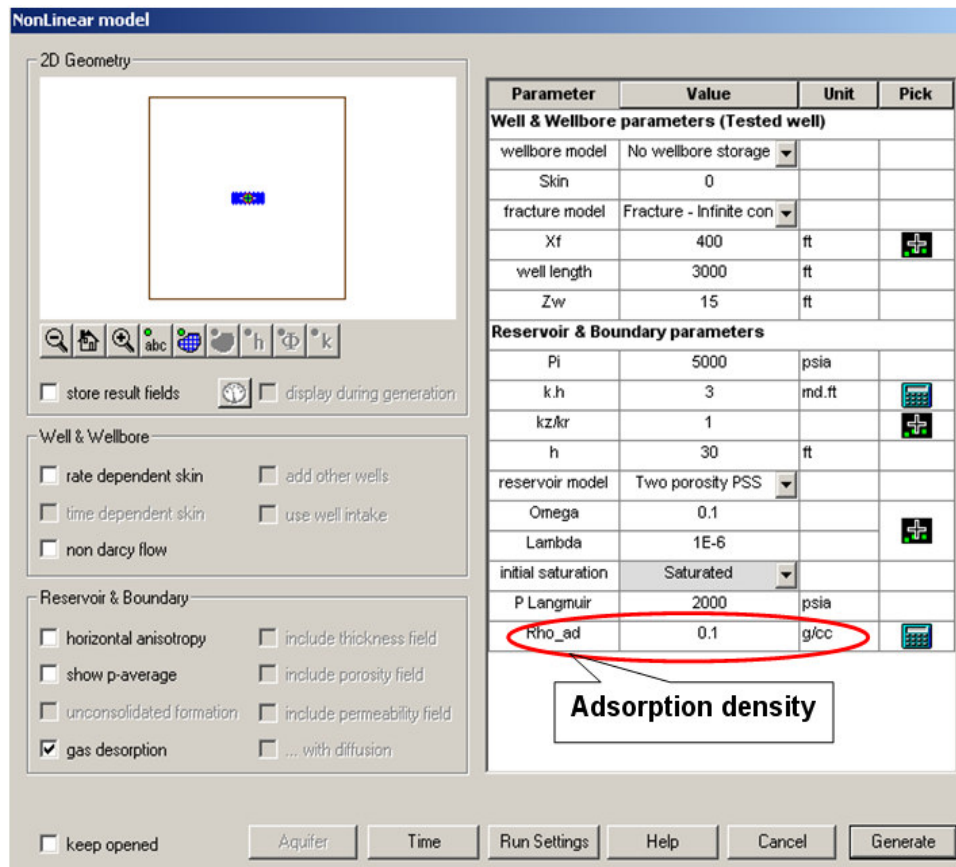
Figure 12. Model Parameter Input Dialog Window of Kappa Ecrin

The adsorption density (noted as ρ_{ads} in Ecrin) is easily related to the Langmuir Volume. Adsorption density is the product of Langmuir volume, adsorbed gas surface density and rock density:

$$\rho_{ads} = \rho_{rock}\rho_{gas}^{surf}V_L \dots\dots\dots\dots\dots\dots\dots\dots\dots\dots\dots\dots\dots\dots\dots\dots\dots\dots\dots\dots (3)$$

Where,

ρ_{ads}, [g/cc], adsorption density;

ρ_{rock}, [g/cc], rock density;

ρ_{gas}^{surf} , [g/cc], adsorbed gas density;

V_L, [cc/g], Langmuir volume;

Gas adsorption density is not a real density but only holds a dimension of density, mass over volume. Usually, Langmuir volume tells the maximum amount of gas that can be adsorbed in terms of the gas volume per unit rock mass. Adsorption density is just converting the Langmuir volume to the gas mass per unit rock volume. The product of Langmuir volume and rock density gives gas volume per unit rock volume, and further multiplying the product by adsorbed gas density gives the gas mass per unit rock volume with a unit of density. The adsorption density is just an equivalent way of expressing Langmuir volume. The only inconvenient issue is the unit conversion. Langmuir volume is usually told with the unit of Standard Cubic Feet per Ton, so the equivalent calculation is:

$$\rho_{ads}[g/cc] = 0.3048^3 \times \rho_{rock}[g/cc]\rho_{gas}^{surf}[g/cc]V_L[SCF/TON] \dots\dots\dots\dots\dots\dots\dots\dots (4)$$

If inputting Langmuir volume and rock density is preferred, the Langmuir volume can be converted into grams per cubic centimeter. Figure 13 shows the dialog window (inside the red circle) for inputting them separately. Adsorption gas density is automatically computed by the software according the input PVT data.
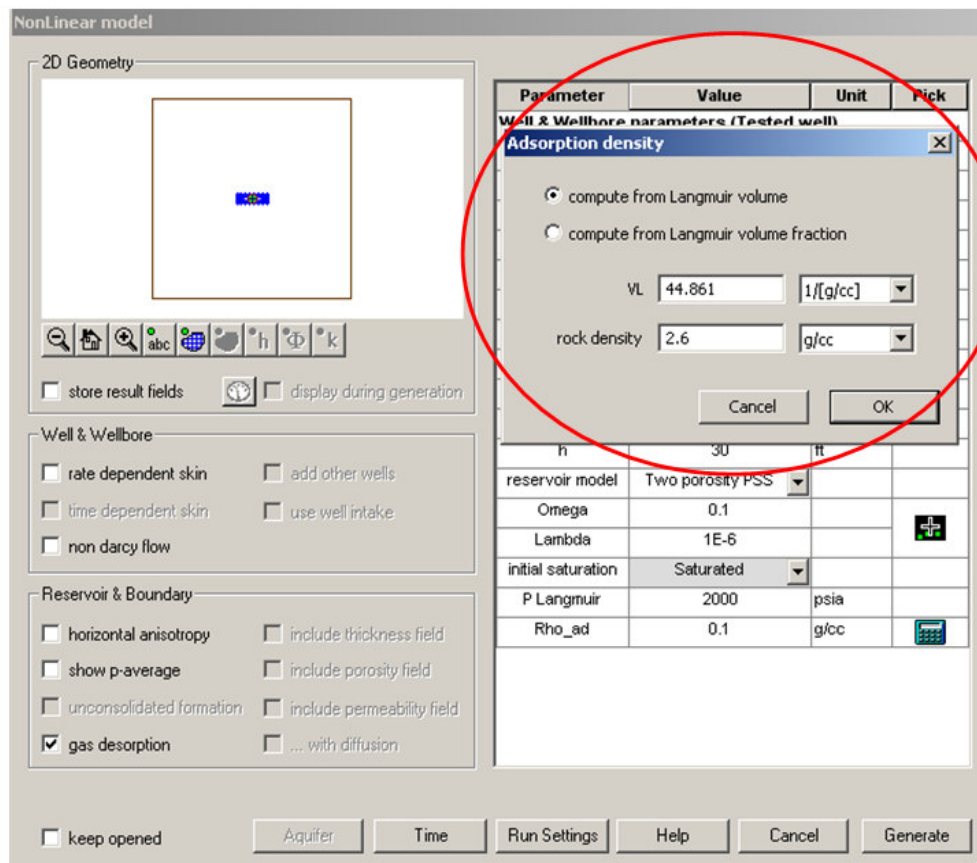
Figure 13. Dialog Window for Inputting Langmuir Parameters in Kappa Ecrin

The Ecrin model assumes instantaneous desorption, and when the adsorption option is selected in the shale gas model, there is no option to enter desorption time in the parameter input dialog window.

This chapter described a conceptual model appropriate for shale gas, and specifically and how gas is stored and flowing. The following chapter will introduce a methodology (Valko 2009) for determining estimated ultimate recovery to shale gas wells and will show EUR estimates for New Albany shale gas wells.

CHAPTER III

RATE DECLINE ANALYSIS FOR NEW ALBANY SHALE GAS WELLS

Production rate data of 33 New Albany Shale gas wells can be used to analyze rate decline behavior of those wells in order to estimate the estimated ultimate recovery. Though other approaches exist for analyzing the rate decline and estimated ultimate recovery (EUR) of wells in gas shales and other unconventional reservoirs, this chapter will apply only the Valko (2009) technique.

3.1 EUR Determination from Rate Decline Analysis

Valko (2009) developed an empirical and mechanical approach for EUR estimation based on the research in production history of 7000 plus wells in Barnett Shale, and the application only requires production rate data.

Eq 5 shows the mathematic expression of the model and Table 1 shows the meaning of each term in this equation.

$$rp = 1 - \frac{Q}{EUR} = 1 - \frac{Q_D}{EUR_D} = \frac{1}{\Gamma(\frac{1}{n})}\Gamma[\frac{1}{n}, -\ln q_D] \dots\dots\dots\dots\dots\dots\dots\dots\dots\dots\dots\dots\dots\dots (5)$$

This is a simple equation combined by two Gamma functions. For each rate data point, we can calculate its recovery potential by assigning a value to *n* parameter. Though the derivation of this model includes another model parameter τ, substituting expressions for q_D, Q_D and EUR_D from Table 1 can make calculation of recovery factor without τ.

Table 1. Valko EUR Estimate Approach Parameters (Valko, 2009)

Variable	Expression	Remark
t	Period, dimensionless (in case of monthly data, the number of months)	
q	Produced gas in period (eg. mscf/month)	
q_i	Model parameter, maximum (or initial) production rate	
n	Model parameter, dimensionless	
τ	Model parameter, dimensionless, 'characteristic number of periods'	
Q	$\int_0^t q\,dt$	Cumulative production
EUR	$\int_0^\infty q\,dt$	Estimated Ultimate Recovery
rp	$1 - \dfrac{Q}{EUR}$	Recovery potential
q_D	$\dfrac{q}{q_i}$	Dimensionless production rate
Q_D	$\dfrac{Q}{q_i}$	Dimensionless cumulative production
EUR_D	$\dfrac{EUR}{q_i}$	Dimensionless EUR
$\dfrac{dq}{dt}$	$-n\left(\dfrac{t}{\tau}\right)^n \dfrac{q}{t}$	Defining differential equation of the model
q	$q_i \exp\left[-\left(\dfrac{t}{\tau}\right)^n\right]$	Rate expression as function of time
q_D	$\exp\left[-\left(\dfrac{t}{\tau}\right)^n\right]$	Dimensionless rate expression
Q_D	$\dfrac{\tau}{n}\left\{\Gamma\left[\dfrac{1}{n}\right] - \Gamma\left[\dfrac{1}{n},\left(\dfrac{t}{\tau}\right)^n\right]\right\}$	Dimensionless cumulative production expression
EUR_D	$\dfrac{\tau}{n}\Gamma\left[\dfrac{1}{n}\right]$	Dimensionless EUR expression
rp	$\dfrac{1}{\Gamma\left[\frac{1}{n}\right]}\Gamma\left[\dfrac{1}{n}, -\ln q_D\right]$	Recovery potential calculated from dimensionless rate

For analyzing production data, following procedure is suggested:

1) Prepare a data series consisting of q_D and Q_D.

2) Assuming a parameter n, calculate recovery potential from Eq 5.

3) Plot of rp versus Q_D. The series should appear as a straight line, as it can be easily

proven by substituting the expressions of q_D and Q_D into Eq 5.

The two intercepts of the straight line are (theoretically):

y-intercept $=1$

x-intercept $= EUR_D$

4) The estimated ultimate recovery can be obtained as the x-intercept of the straight line.

5) The actual y–intercept can be compared to the theoretical value (that is unity). If the y–intercept is not equal to 1, the parameter n should be adjusted.

Figure 14 shows the application of the above producer for New Albany shale gas well Well A. By assigning a random value for the n parameter, we can calculate the recovery potential for each data point, and plot recovery potential versus the corresponding dimensionless cumulative production. The n parameter is adjusted until we get all the points to lie on a straight line with unit y-intercept. For Well A, $n=0.57$ is the value that best satisfied these criteria. Then the dimensionless EUR is determined from as the x-intercept, 250 (not shown in the graph). Ultimately, $EUR= EUR_D \times q_i$ $=123750$MSCF.

Valko Model for recovery potential estimation

$y = -0.004x + 1$
$R^2 = 0.5055$

parameters	values
Well #	Well A
Initial rate, mscf/d	531
Optimal n	0.57
Slope absolute value	0.004
Maximum Square-R	0.5055
X-intercept	250
EUR , mscf	132750
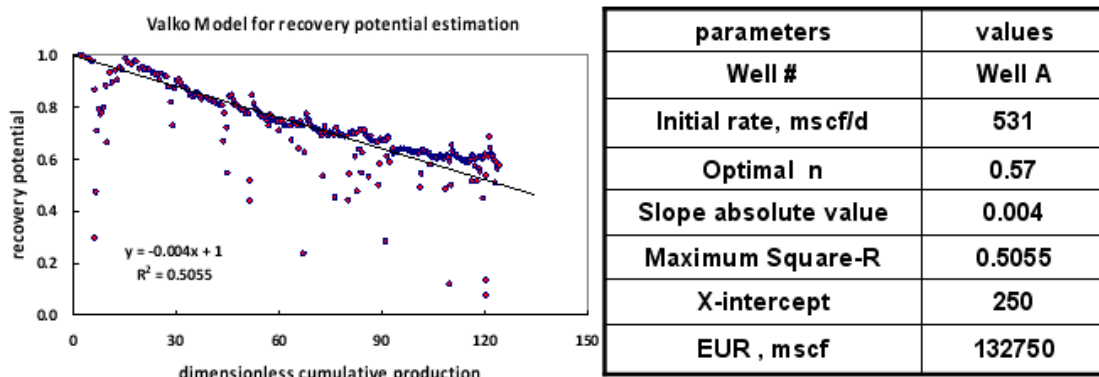
Figure 14.EUR Estimation of Well A by Valko Approach

3.2 EUR Estimates for New Albany Shale Gas Wells

We applied Valko Approach to 33 wells in New Albany Shale gas wells. EUR estimation result is shown in Figure 15.

Valko Model for EUR estimation
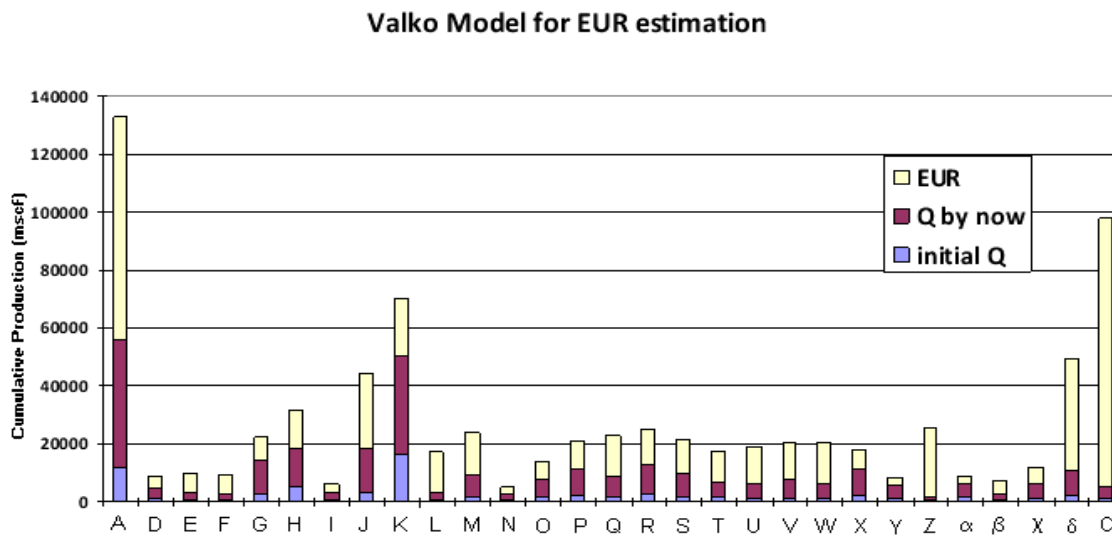
Figure 15. EUR Estimation of 33 Wells in New Albany Shale

From the EUR estimates of these 33 wells, we find though the EUR varies considerably from well to well, and some of the wells still have considerable recovery potential. Well A and Well C are multi-fracture horizontal wells, and they indicate much higher recovery potential, as might be expected because the fractures provide much more contact with the shale.

The next chapter investigates the relationship between reservoir contact and long term production.

CHAPTER IV

DRAWDOWN PRESSURE TRANSIENT BEHAVIOR IN MULTI-TRANSVERSE FRACTURED HORIZONTAL WELLS (MTFHWS)

This Chapter will focus on the drawdown PTA behavior of horizontal wells with multiple transverse fractures. The reason why this special well type is now widely used in shale gas development will be explained. Some previous model for MTFHWs will also be described. We will explain the rationale of using long term drawdown model behavior to reveal more information from production data. We will explain two methods for analysis of long-term production data: Rate-Normalized Pressure (RNP) Analysis and unified BU-RNP analysis. A sensitivity study helps illustrate long-term drawdown behavior of MTFHW in shale gas reservoir, and flow regime behavior will be discussed. Additionally, we will also shed light on the impact of gas desorption on the long-term drawdown behavior of the MTFHW. We will emphasize the implications of the early linear flow regime that are fundamentally important to shale gas well design.

4.1 MTFHWs in Shale Gas Reservoirs

The success of development of gas shales is dependent on recent technological advances in two key technologies: horizontal drilling and hydraulic fracturing (Arthur, Bohm and Layne, 2008). The combination of these two technologies realizes the economic gas production in gas shales. However, the importance of horizontal drilling and hydraulic fracturing was not learned in just one day.

The first commercial oil well was drilled in Ignacy Lukasiewicz, Poland in 1853 and the first oil well in United States, which is known as the famous "Drake Well" was drilled at Titusville, Pennsylvania after 6 years. As the petroleum industry developed, hydraulic fracturing was applied during 1940's. Hydraulic fracturing for stimulation of oil and natural gas wells was first used in the United States in 1947 and first used commercially in 1949. Because of its success in increasing production it was quickly adopted, and is now used worldwide in tens of thousands of oil and natural gas wells annually.

The first recorded true horizontal well, drilled near Texon, Texas, was completed in 1929. During 1980's decade, horizontal drilling technology brought a revolution to petroleum industry. Soon that horizontal drilling has become a standard industry practice (Arthur, Bohm and Layne, 2008).

Since the inception of fracturing of horizontal wells in late 1980's, several field cases , for example, Lost hills Diatomite in California, upper Behariyia reservoir in Egypt and gas production in Australia, have been reported (Wei and Economides 2005). Two limiting cases exist in usual fracturing horizontal well: the longitudinal and the transverse (Figure 16). The former case means the well is drilled along the expected fracture trajectory while the later means the well and fracture face are perpendicular to each other. However, the industry reports of application of horizontal well fracturing indicated transverse case dominates (Wei and Economides 2005).
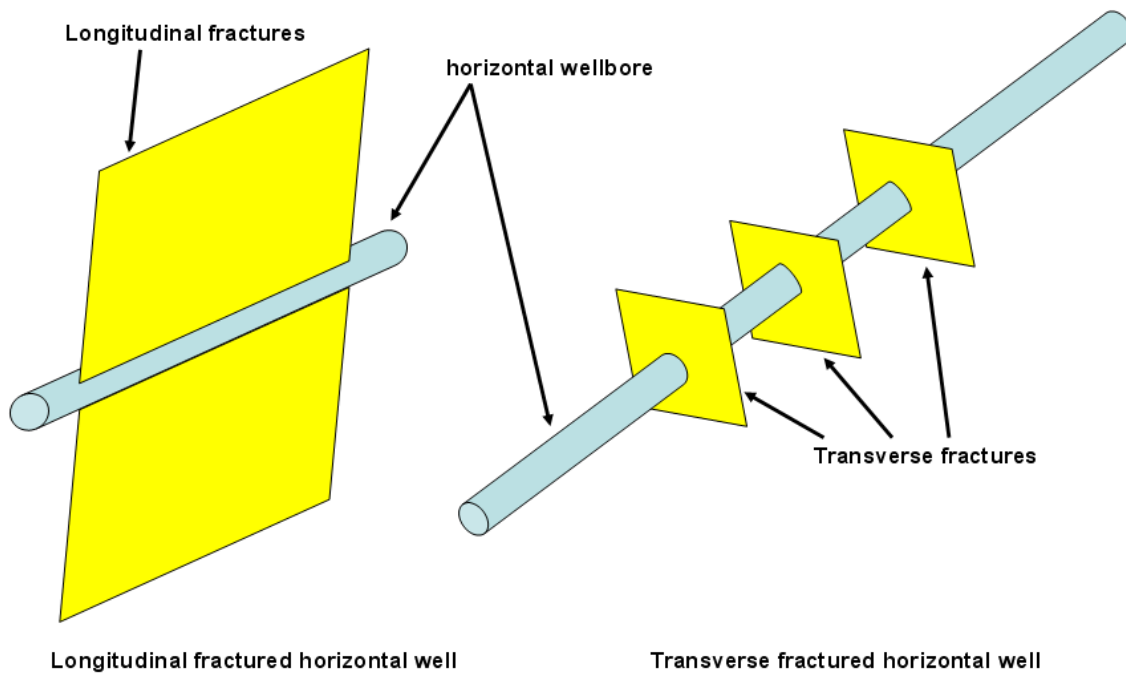
Figure 16. Illustration of Longitudinal and Transverse Fractures in Horizontal Wells

Horizontal wells with multiple transverse hydraulic fractures are believed to be the strategy for economic gas production in shale gas plays. The industry prefers MTFHWs because they can optimize the contact between the reservoir and the wellbore. The multi-stage fracture treatments in horizontal wellbores create a large stimulated reservoir volume (SRV) that increases both production and estimated ultimate recovery (EUR) (Meyer *et al* 2010).

4.2 Previous Models for MTFHWs

Freeman *et al* (2009) developed a numerical model to study the performance of MTFHWs in tight gas and shale gas reservoir system. This numerical model takes gas desorption into account and applies finite-conductivity fracture model. Simulation results reveal the reservoir flow regimes by pressure profiles shown as Figures 17, 18 and 19 in order.
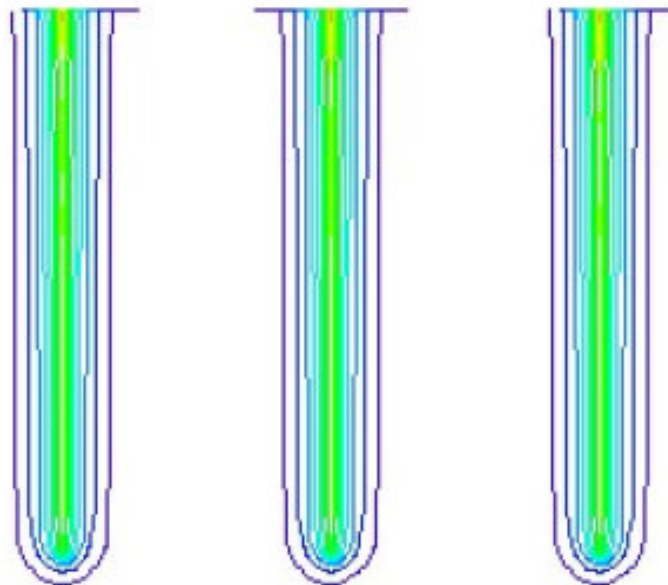
Figure 17. Pressure Profile: Half Reservoir, Linear Flow Normal to Fractures (Modified From Freeman *et al* 2009)
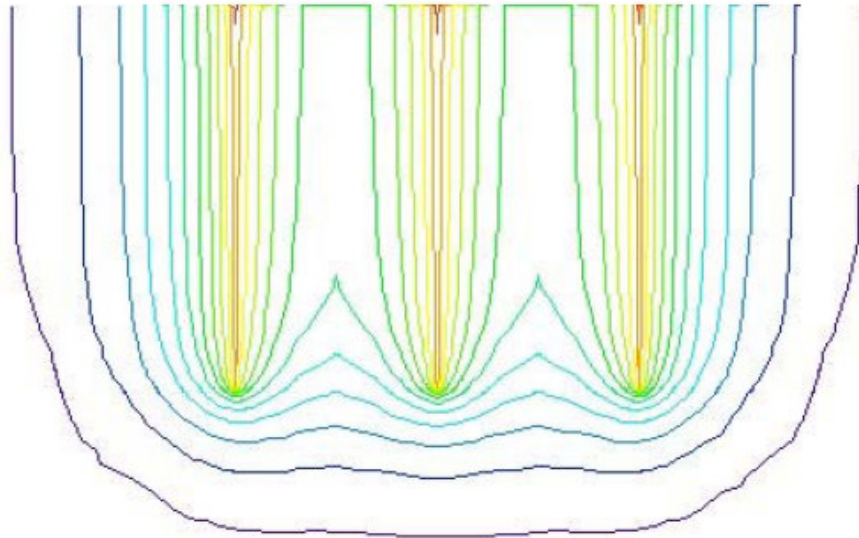
Figure 18.Pressure Profile: Half Reservoir, Compound Linear Flow

(Modified From Freeman *et al* 2009)
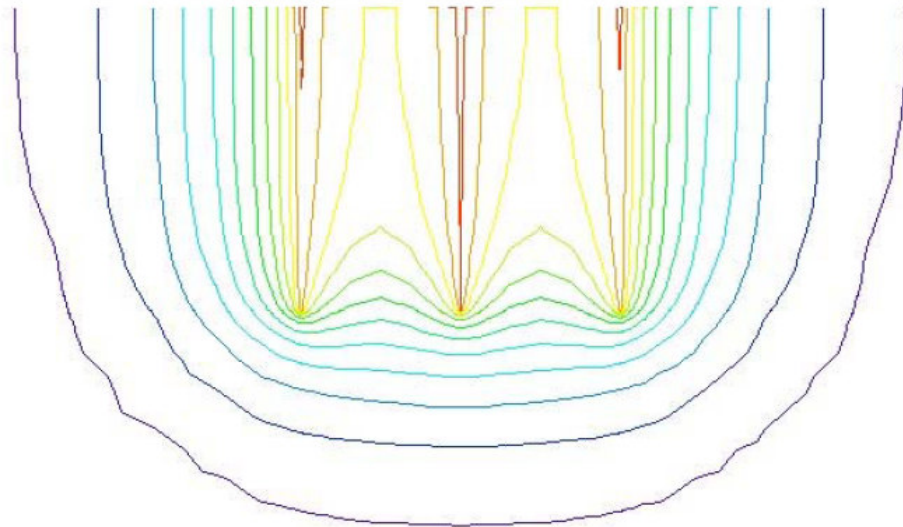
Figure 19.Pressure Profile: Half Reservoir, Elliptical Flow

(Modified From Freeman *et al* 2009)

Also, Freeman *et al* (2009) also plotted the normalize rate derivative function

respect to square root of time versus time for both infinite reservoir case and finite

reservoir case to reveal the flow regimes (Figure 20). The normalized rate derivative

function (square root of time basis) is defined as Eq (6):

$$\frac{d(1/q)}{d\sqrt{t}}$$ …………………………………………………………………………. (6)

(Note: this definition should be under the precondition that production is performed with

constant well bottom pressure)
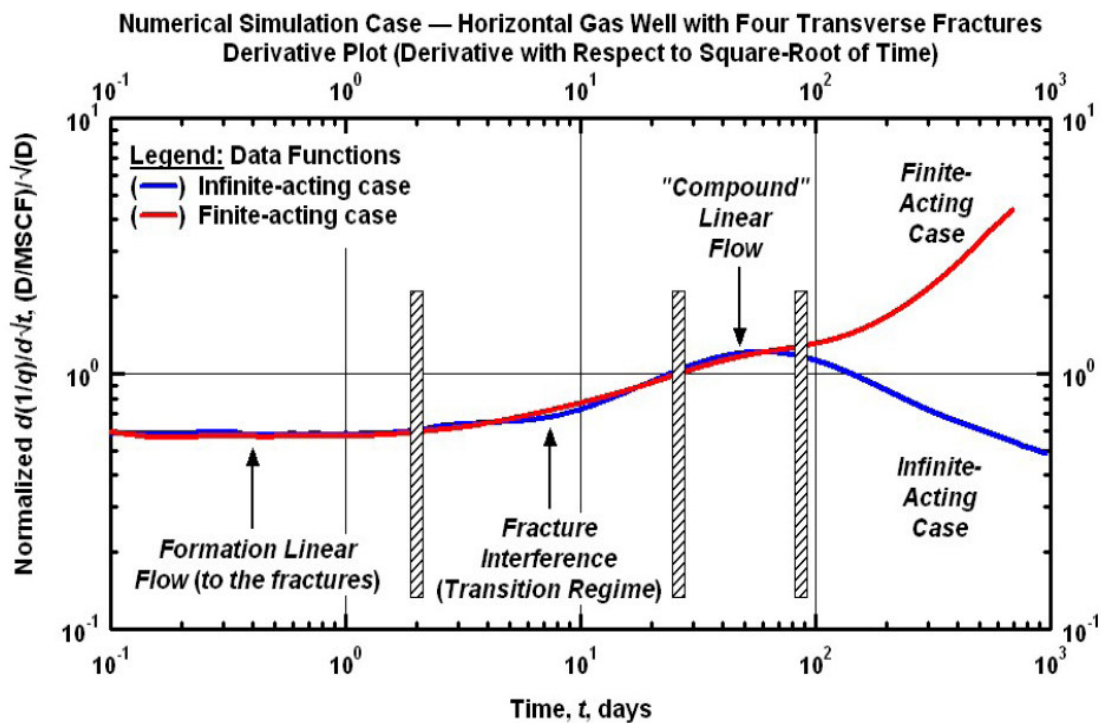
Figure 20. Boundary & Fracture Interference on Normalized Rate Derivative Function

(Freeman *et al* 2009)

Al-Kobaisi *et al* (2006) also established an analytical model to study the pressure transient behavior of MTFHWs with finite-conductivity fractures. By solving the analytical partial differential equation, potential flow regimes of MTFHWs are revealed as Figure 21.
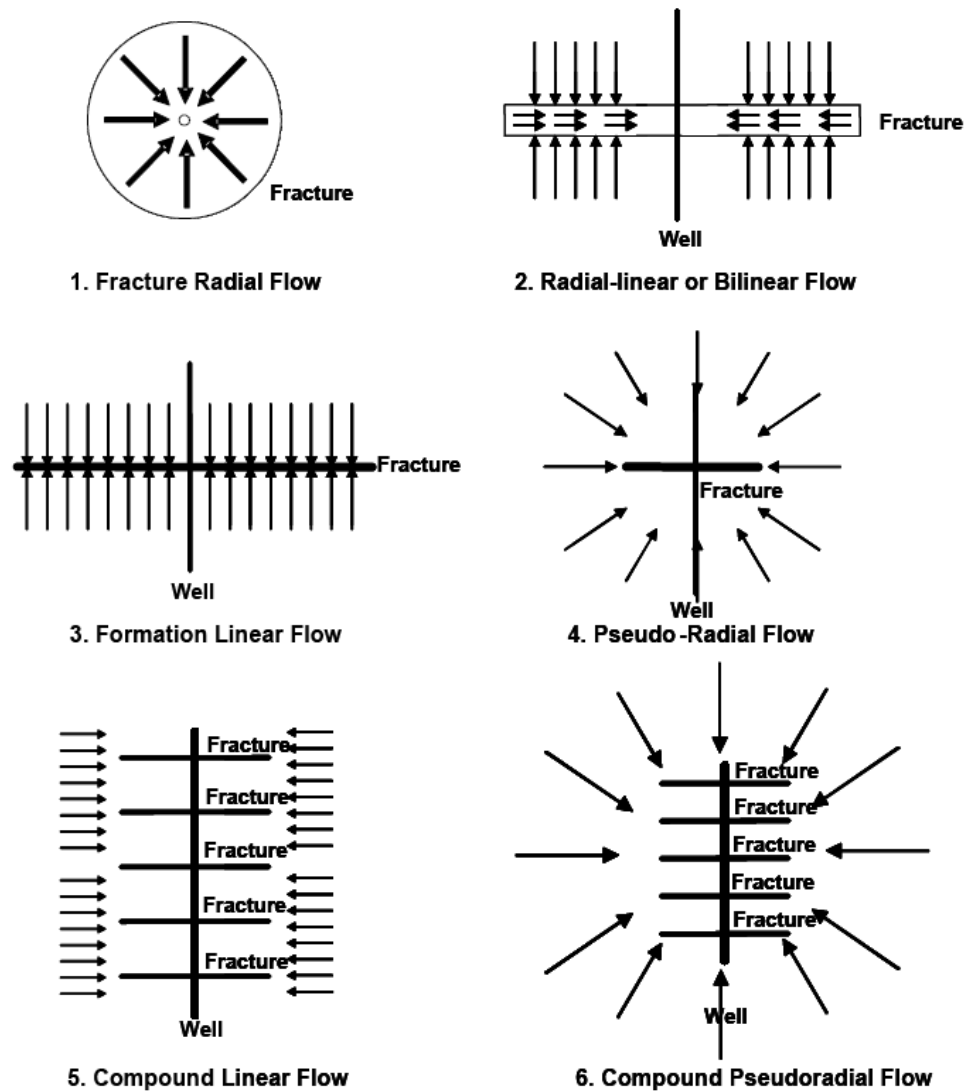
Figure 21. Potential Flow Regimes Identified in MTFHWs (Al-Kobaisi *et al* 2006)

Clarkson *et al* (2009) also studied the flow regime issue in the view of production data analysis through the normalized rate derivative function. First, they define the term "adjust time function" t^*. The specific meaning of t^* can be set as real time (t), adjust pseudotime (t_a^* defined as Eq 7) or adjust material balance time (t_{ca}^* defined as Eq 8).

$$t_a^* = (\mu_g c_t^*)_i \int_0^t \frac{1}{\overline{\mu_g c_t}^*} dt \dots\dots\dots\dots\dots\dots\dots\dots\dots\dots\dots\dots\dots\dots\dots\dots\dots\dots\dots\dots\dots \quad (7)$$
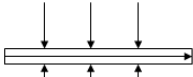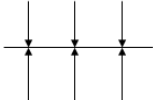
$$t_{ca}^* = \frac{(\mu_g c_t^*)_i}{q_g} \int_0^t \frac{q_g}{\overline{\mu_g c_t}^*} dt = \frac{(\mu_g c_t^* Z^*)_i}{q_g} \frac{G_i}{2 p_i} [m(p_i) - m(p_r)] \dots\dots\dots\dots\dots\dots\dots\dots\dots \quad (8)$$

Both Eqs. 7 and 8 include the altered variables c_t^* and Z^* those accounts for desorption. These variables assume instantanesous desorption, which is a reasonable assumption for long-term production in several commercial shale and coalbed methane reservoirs (Clarkson *et al* 2009). The definition of adjust time and material adjust time include the consideration of desorption through these altered variables. However, the advantage of t_{ca}^* compared to t_a^* is that it can be applied in variable rate/flowing pressure scenario while t_a^* is just for constant flowing bottomhole pressure. The flow regimes can be identified by the characterization of normalized rate derivative on a log-log diagnosis plot. Different form of the normalized rate derivative function will give different appearance of the curve, as Table 2 shows, but they represent the same flow regimes.

For the MTFHW case, they provided a brief illustration to reveal all the potential flow regimes (Figure 22).

Table 2. Flow Regime Identification Scheme by Normalized Rate Derivative Function (Modified from Clarkson *et al* 2009)

Flow regimes	Log-Log diagnostic	Plot	Derivative function characterization
Bilinear flow	Radial derivative	$\dfrac{m(p_i)-m(p_{wf})}{q_g} \, vs. \log(t^*)$	1/4 slope
	Bilinear derivative	$\dfrac{m(p_i)-m(p_{wf})}{q_g} \, vs. \sqrt[4]{t^*}$	0 slope
Linear flow	Radial derivative	$\dfrac{m(p_i)-m(p_{wf})}{q_g} \, vs. \log(t^*)$	1/2 slope
	Linear derivative	$\dfrac{m(p_i)-m(p_{wf})}{q_g} \, vs. \sqrt[2]{t^*}$	0 slope
Radial flow	Radial derivative	$\dfrac{m(p_i)-m(p_{wf})}{q_g} \, vs. \log(t^*)$	0 slope
No-flow boundary flow (Pseudo-Steady State)	Radial derivative	$\dfrac{m(p_i)-m(p_{wf})}{q_g} \, vs. \log(t^*)$	1 slope
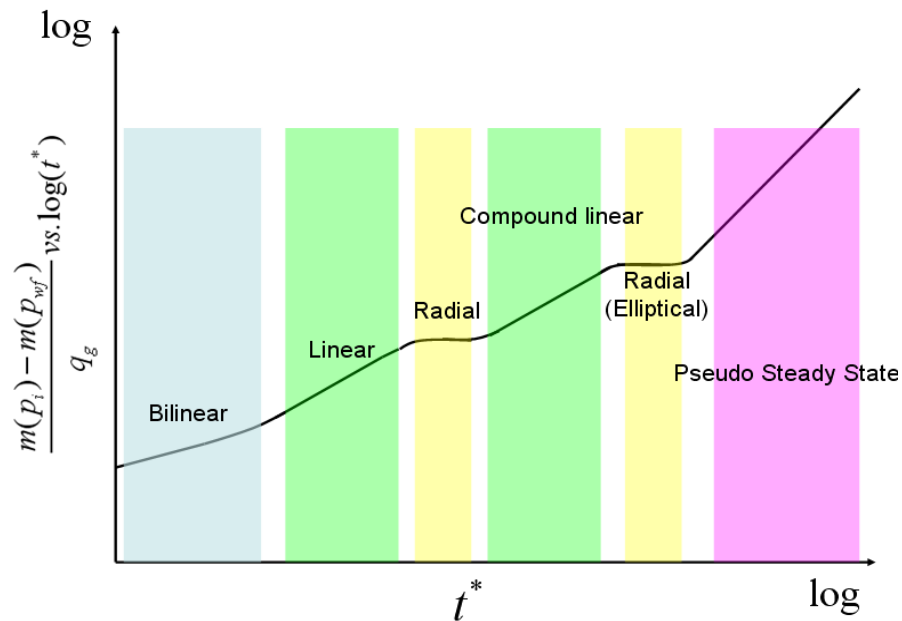
Figure 22. Potential Flow Regimes in MTFHW (Finite Conductivity Fractures)

Previous study of MTFHWs' model provided support for understanding the flow regimes of MTFHWs. Though the models study mentioned above are from different ways, including numerical model (Freeman *et al* 2009), PTA analytical (Al-Kobaisi *et al* 2006) model and production data analysis (Clarkson *et al* 2009), we can still capture a basic image of flow regimes of MTFHWs, especially reservoir flow regimes.

4.3 Rationale for Use of Long Term Drawdown Model Behavior

Models for long term rate decline behavior at a constant pressure and those for pressure drawdown at a constant production rate have been maturely developed. Matching a long term rate decline behavior or pressure drawdown behavior against an appropriate model is an effective way to diagnose well and reservoir characteristics.

However, usually neither of rate and pressure data is constant in reality. Therefore, to perform analysis to the data with the existing long term drawdown models, we need to process the varying rate and varying pressure data into a virtual long term rate decline behavior at constant pressure or a virtual pressure drawdown behavior at constant rate.

4.3.1 Rate-normalized Pressure Analysis as Alternative to Rate Decline Analysis

In reality, the rate and pressure data recorded during the production of a well are both varying. Palacio and Blasingame (1993) provided a way to view long term production data as a single virtual rate decline at constant pressure. The graph of the instantaneous productivity index as a function of material balance time computed as the cumulative production over the last rate provides a virtual constant pressure rate decline, and this enables matching against rate decline model that represent the same well and reservoir characteristics as can be modeled for constant rate drawdown. But rate decline behavior is not as straightforward to diagnose as pressure drawdown behavior for constant rate production, which shows readily identified straight trends with characteristic slope when viewed as pressure change derivative. Therefore, we use RNP analysis to provide a virtual constant rate pressure drawdown for a well produced at variable rate and variable pressure, and it enables matching against pressure drawdown models, which is more straightforward than rate decline model for diagnosing well and reservoir characteristics (Ehlig-Economides, Martinez Barron and Okunola 2009).

Rate-normalized pressure (RNP) is simply the reciprocal of the instantaneous productivity index (Eq 9), and its derivative is defined as Eq 10. It provides virtual

constant rate drawdown behavior for arbitrary variations in rate and wellhead pressure.

$$RNP = \frac{p_i - p_{wf}}{q} \dots\dots\dots\dots\dots\dots\dots\dots\dots\dots\dots\dots\dots\dots\dots\dots\dots\dots\dots\dots\dots\dots (9)$$

$$RNP' = \frac{dRNP}{d\ln t_e} = \frac{d\,(p_i - p_{wf}/q)}{d\ln t_e} \dots\dots\dots\dots\dots\dots\dots\dots\dots\dots\dots\dots\dots\dots\dots\dots (10)$$

(Note: RNP' can be modified as RNP's derivative with respect to elapsed time rather

than material balance time to avoid superposition effect, as discussed in Paper SPE

123042 (Ehlig-Economides, Martinez Barron and Okunola 2009)).

Plotting RNP and RNP' versus material balance time on log-log coordinate can

shed lights on well behavior and flow regimes. In Ecrin Topaze this plot is also produced

when rate and pressure data is input.

4.3.2 Unified BU-RNP Analysis

Pressure transient analysis (PTA) is also performed to analyze the well behavior

as well as PDA. Moreover, build-up tests are preferred in the industry. However, Due to

the difference in data collection between PTA and PDA, these analyses are performed

independently, yielding multiple interpretations from a diverse group of people and

software programs. At times the results may conflict, and creating one consistent well

and reservoir characterization can be quite challenging and time consuming. A unified

interpretation of both analyses would reduce analysis time and increase confidence in the

results (Ehlig-Economides, Martinez Barron and Okunola 2009).

The unified BU-RNP method (Ehlig-Economides, Martinez Barron and Okunola

2009) provides a more complete analysis than either PTA or PDA alone can provide by

combining relatively short-duration PTA data and long-term PDA data. The essence of this processing is also to transferring a production process into a virtual constant-rate drawdown behavior that can be diagnosed like pressure and pressure derivative and matched against an appropriate model, but compared to pure RNP analysis this method considers both PDA and PTA (selected build up) and makes the analysis more trustable.

To perform unified BU-RNP method, the following main steps should be performed:

1. Selected a build up part, calculate pressure change and its derivative with respect to elapsed time, and back-integrate it into a drawdown behavior. The result will provide early behavior of the final unified plot.

2. Assign a constant rate used for multiplying RNP in order to combine RNP with BU in the future, and transfer PDA data into a virtual pressure drawdown behavior under this constant rate through RNP processing (there are sub-steps for deleting the redundancy (Ehlig-Economides, Martinez Barron and Okunola 2009)). This will provide the long term response of the unified plot.

3. Combine the results from PTA and PDA as the whole virtual drawdown [If the result from PDA contains the data sharing the same time domain with the result from PTA, the PTA is used because it is usually smoother, but it is also subject to superposition distortion. Overlapping the two response trends to throw off nonlinear regression in automated matching].

4. Analyze the unified plot and find an appropriate drawdown model to match it.

The procedure will also be instructed while it is applied to analyze the field case in the future chapter.

4.4 Sensitivity Studies Illustrating Long Term Drawdown Behavior of MTFHWs in Shale Gas Reservoirs

To illustrate the long term drawdown behavior of MTFHWs in shale gas reservoirs, we run a series of sensitivity studies. The sensitivity is performed to permeability. Table 3 lists the well, reservoir and PVT properties, and Table 4 shows the model settings. Table 5 lists the specific sensitivity cases we run.

We run three series of cases, each series represents one boundary condition (No flow boundary, infinite reservoir and constant pressure boundary). In each series, a sensitivity study to permeability ranging from 0.0001 md to 1 md is performed.

Table 3. Well, Reservoir and PVT Settings for Sensitivity Study

Reservoir settings		
Reservoir type	Gas shale	
h, ft	Pay zone thickness	30
ϕ	Porosity	0.1
T, ºF	Reservoir temperature	212
p_i, psia	Initial reservoir pressure	5000
Well and stimulated fracture settings		
well type	Multi-transverse fractured horizontal well	
L, ft	Well length	3200
n_f	Number of fractures	8
x_f, ft	Half length of fractures	1200
r_w, ft	Wellbore radius	0.3
z_w, ft	well vertical distance to reservoir bottom	15
PVT settings		
γ_g	Gas specific gravity	0.7

Table 4. Model Settings for Sensitivity Study

Well and wellbore parameters		
Wellbore model	No wellbore storage	
s	Skin factor	0
Fracture model	infinite-conductivity	
Reservoir parameters		
k_z/k_r	vertical/horizontal permeability anisotropy	1
Reservoir model	Homogeneous	
Desorption settings		
Adsorption saturation	Saturated	
p_L, psia	Langmuir pressure	2000
ρ_{ads}, g/cc	Adsorption density	0.1
Production design		
t_p, hr	Production time	1.00E+08
q, Mscf/d	Gas production rate	100

Table 5. Sensitivity Study Cases

Case name	Boundary condition	Permeability (md)
MTFHW_NF_k= 0.0001	No-flow boundary	0.0001
MTFHW_NF_k= 0.001	No-flow boundary	0.001
MTTHW_NF_k= 0.01	No-flow boundary	0.01
MTFHW_NF_k= 0.1	No-flow boundary	0.1
MTFHW_NF_k= 1	No-flow boundary	1
MTFHW_IA_k= 0.0001	Infinite reservoir	0.0001
MTFHW_IA_k= 0.001	Infinite reservoir	0.001
MTFHW_IA_k= 0.01	Infinite reservoir	0.01
MTFHW_IA_k= 0.1	Infinite reservoir	0.1
MTFHW_IA_k= 1	Infinite reservoir	1
MTFHW_CP_k= 0.0001	Constant pressure boundary	0.0001
MTFHW_CP_k= 0.001	Constant pressure boundary	0.001
MTFHW_CP_k= 0.01	Constant pressure boundary	0.01
MTFHW_CP_k= 0.1	Constant pressure boundary	0.1
MTFHW_CP_k= 1	Constant pressure boundary	1

Figures 23, 24 and 25 separately shows the 2-D maps of each series of cases, and Figures 26, 27 and 28 show their corresponding log-log plot of the drawdown behavior in order.
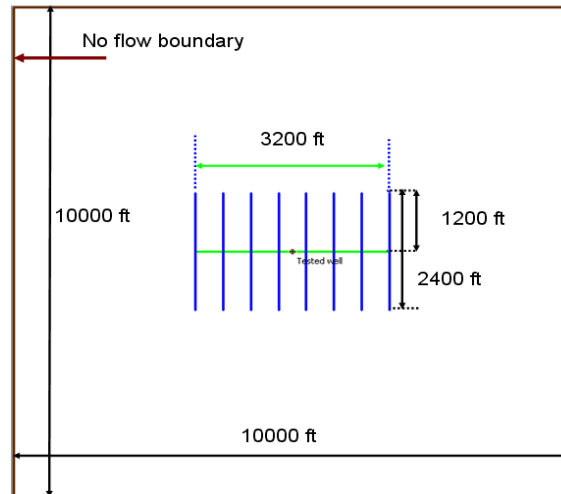
Figure 23. Reservoir and Well Geometry of MTFHW_NF Test Series
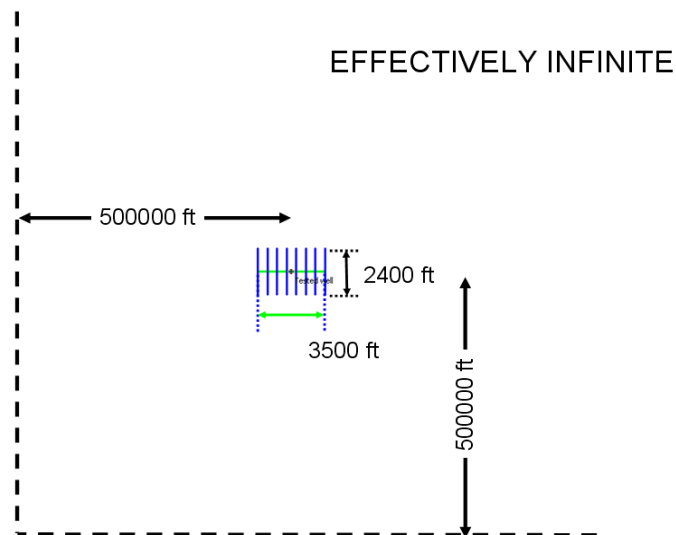
Figure 24. Reservoir and Well Geometry of MTFHW_IA Test Series
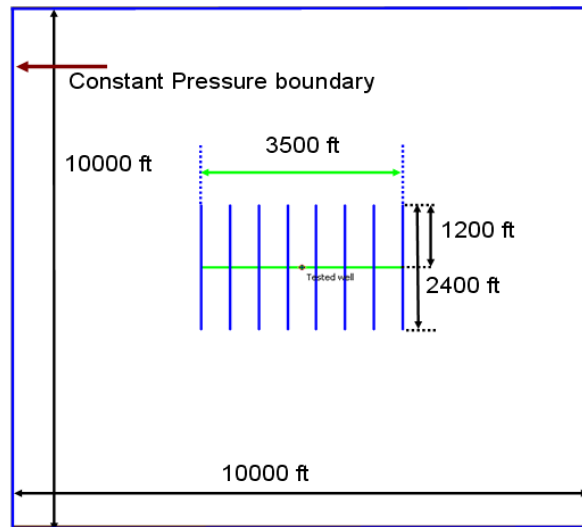
Figure 25. Reservoir and Well Geometry of MTFHW_CP Test Series
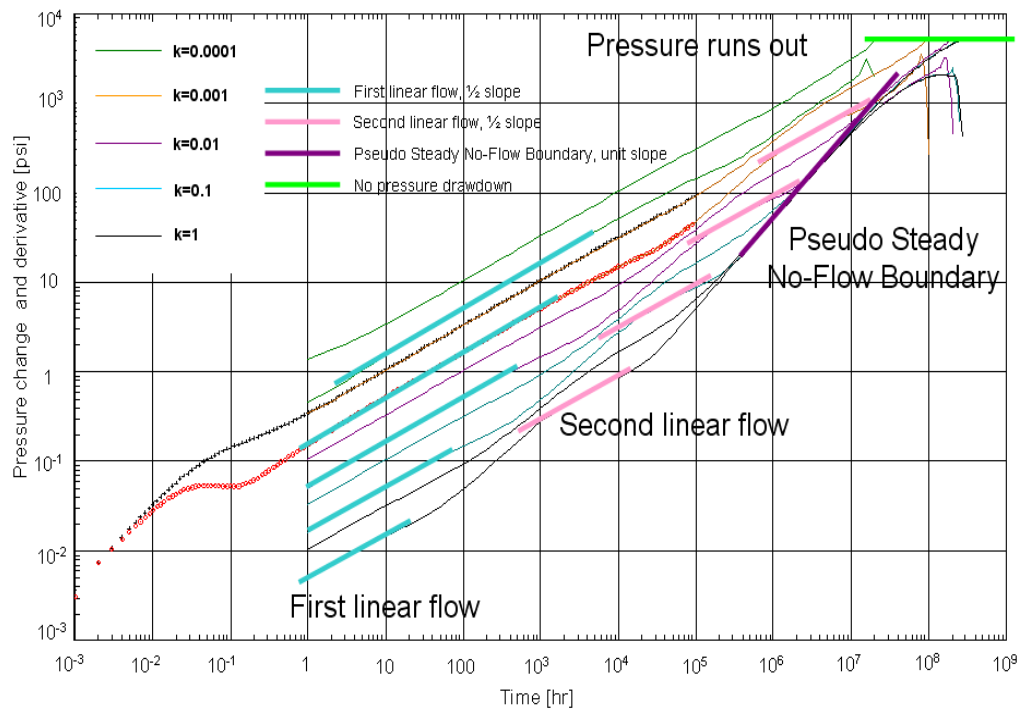
Figure 26. PTA diagnosis plot for MTFHW_NF Test Series
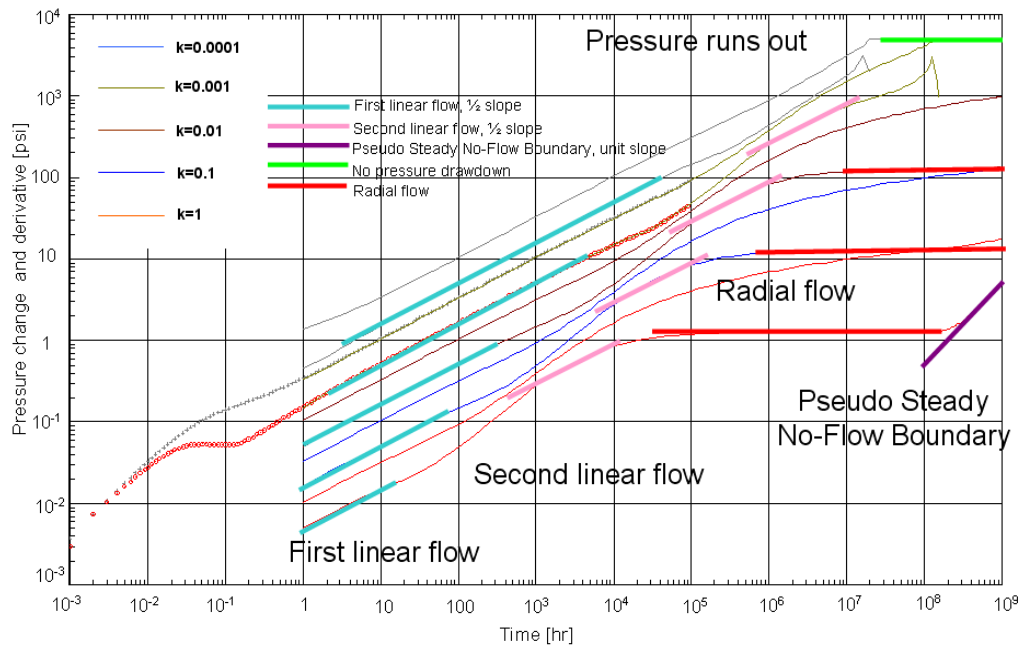
Figure 27. PTA diagnosis plot for MTFHW_IA Test Series
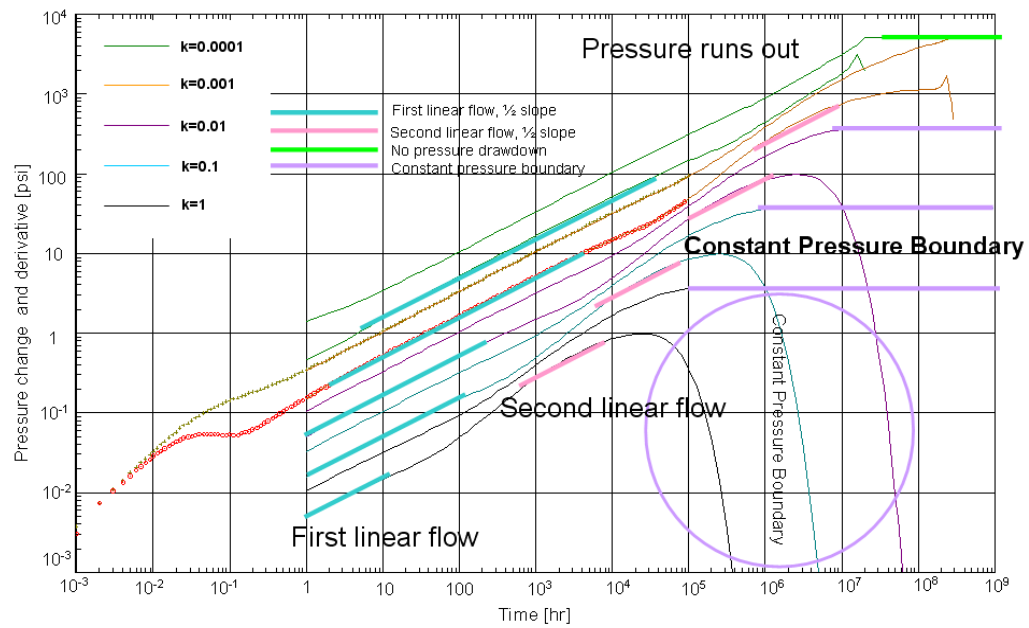
Figure 28. PTA diagnosis plot for MTFHW_CP Test Series

4.4.1 Fracture Storage

Fracture storage effect is identified by the unit slope of pressure change and pressure change derivative at very early time. On each diagnosis plot, the case of k=0.001 md shows the fracture storage effect. The fracture storage effect appears very early and usually lasts a very short time. As reservoir permeability increases, the fracture storage effect will last even shorter time and be replaced by the early reservoir flow regime sooner. Fracture storage is actually a model artifact that appears because Ecrin is using a numerical model that arbitrarily makes all fracture widths 1 cm. We should expect wellbore storage to dominate early time behavior, but this was left out of the sensitivity studies to avoid making behavior of interest.

4.4.2 Early Linear Flow

The first apparent flow regime we observed from the diagnostic plot is linear flow represented by a half-slope derivative (for linear flow, pressure change curve is also half slope). This trend is marked by light blue straight line for each case. This flow regime is the linear flow from reservoir normal to every transverse fracture (Figure 29). Since we use infinite-conductivity fracture model instead of finite conductivity fracture model, which was applied in the previous MTFHW model mentioned in Section 4.2, it is not hard to understand why we don't see bilinear flow before we see this early linear flow. With shale permeabilities in the nanodarcy range, effectively infinite conductivity fractures can be expected.
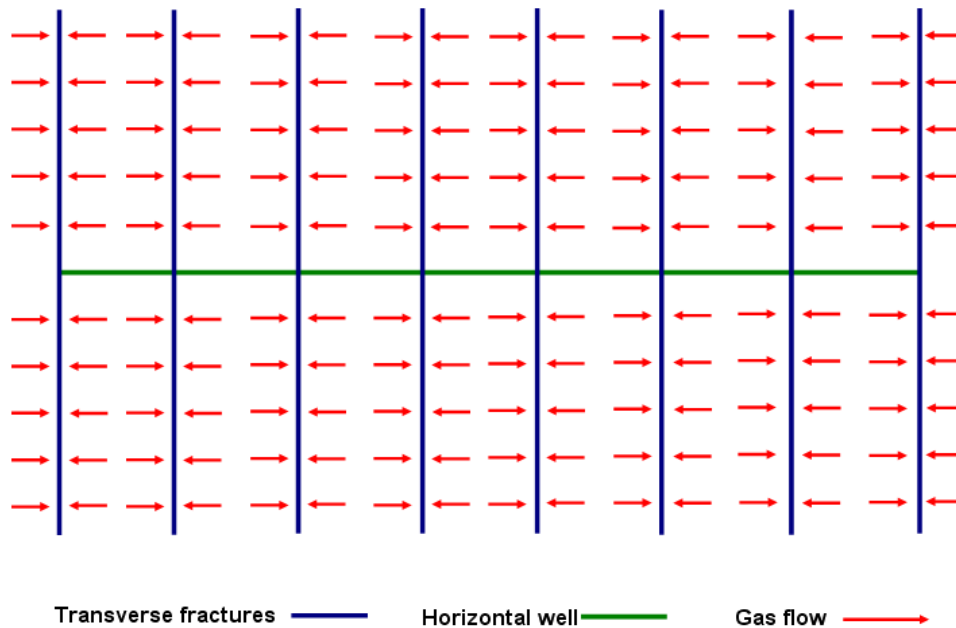
Figure 29. Illustration of the Early Linear Flow Normal to Transverse Fractures

4.4.3 Interference between Adjacent Fractures

As production continues, pressure investigation will travel further into the formation. At some time point, the pressure disturbance front between two adjacent transverse fractures will touch each other so that pressure interference will occur (Figure 30). This is also illustrated on our log-log plots. For each case, derivative curve will bend up at certain time point after the early linear flow, and the derivative departs from the one half slope trend. This interference occurs increasingly earlier with increasing permeability.
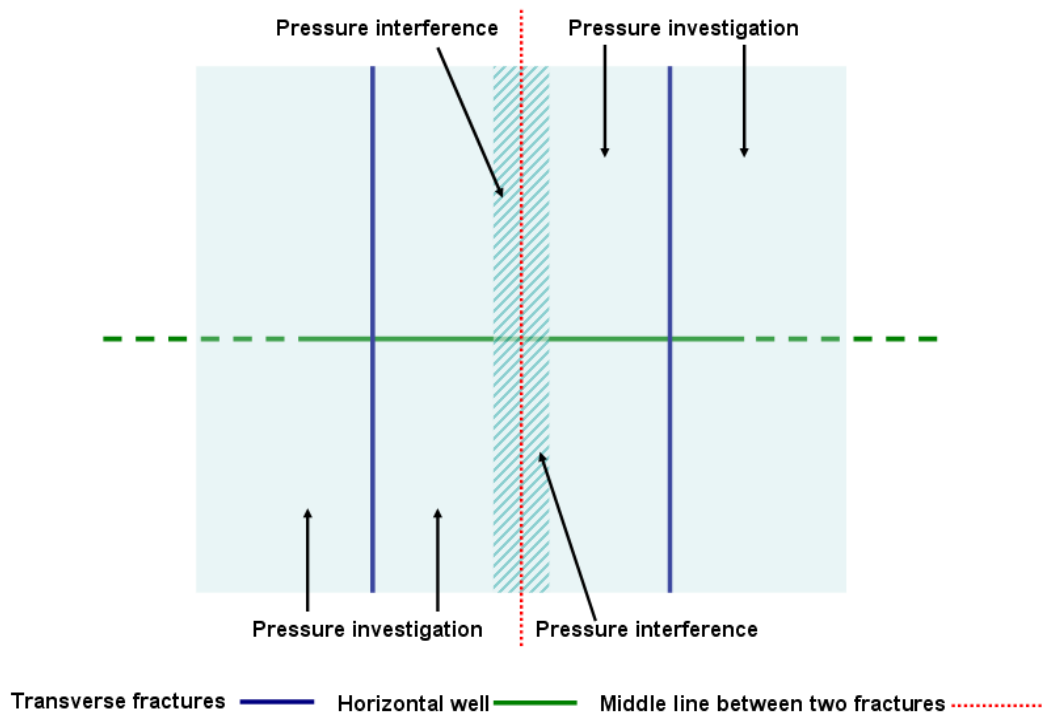
Figure 30. Pressure Interference between Two Adjacent Transverse Fractures

4.4.4 Compound Linear Flow

After pressure interference between two adjacent transverse fractures occurs, the pressure disturbance will cover all the stimulated reservoir volume (SRV) and extend beyond the extent in a flow regime called "compound linear flow" (Figure 31). This flow regime will is represented by the second half-slope derivative trend on the log-log plot. In our sensitivity study, we use pink straight line to mark this flow regime. This flow regime is not a pure linear flow but dominated by linear flow normal to the horizontal well. The flow on the two sides of the wellbore behaves like an elliptical shape, but its impact is weaker than the linear flow normal to the wellbore. The other characterization

of compound linear flow is that on the log-log plot, it lasts less than one square cycle, while early linear flow lasts more than two cycles for permeability less than 0.1 md.
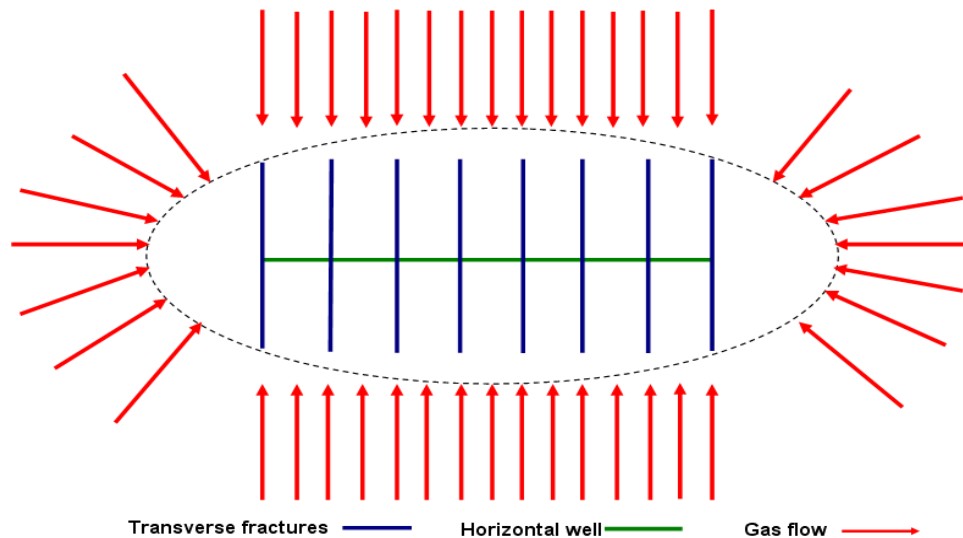
Figure 31. Compound Linear Flow Regime (Modified From Van Kruysdijk *et al* 1989)

4.4.5 Boundary Behavior

After compound linear flow, the pressure investigation may travel even further around the MTFHW system. Based on the reservoir geometry and boundary condition, we saw three kinds of following regime: pseudosteady state (no flow boundary behavior, pressure change and derivative overlap and trend unit slope, marked by violet straight line in Figure 26), infinite acting (infinite reservoir behavior, derivative curve is flat, marked by red straight line in Figure 27) and constant pressure response (constant pressure boundary behavior, pressure change curve is flat and derivative curve descends steeply, marked by the lavender circle and straight line in Figure 28).

Through our sensitivity study, we can conclude a general understanding of flow regimes of MTFHWs in shale gas reservoirs. After the fracture storage effect, which likely will be masked by wellbore storage in field PTA data, early linear flow normal to transverse fractures will form. At some time, the pressure interference between two adjacent transverse fractures occurs, at which time the pressure disturbance will cover the whole stimulated reservoir volume. After that, the pressure investigation extends beyond the SRV and compound linear flow forms. Further, boundary response will occur based on the specific well and reservoir boundary geometry and boundary condition. Figure 32 shows the potential flow regimes in order.

Before the boundary response, all the behaviors of the three studies are identical. For typical shale reservoirs, the permeability of nanodarcy scale might encounter a boundary response only after hundreds of years. Hence boundary behavior is not likely to be seen. In reality, early linear flow normal to transverse fractures might be the only essential flow regime to MTFHWs in shale reservoirs depending on the fracture spacing. The MTFHW may just produce gas within a small distance around transverse fractures and we will not even see the pressure interference and compound linear flow regime for many decades.
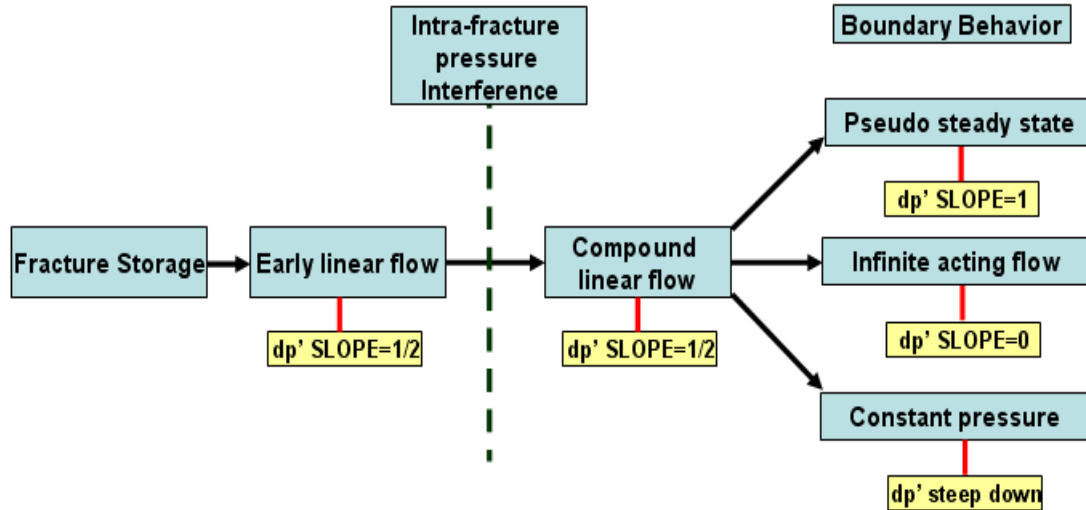
Figure 32. Flow Regimes Revealed through Sensitivity Study

4.5 Impact of Gas Desorption on the Long Term Drawdown Behavior of the MTHWF

The main impact of gas desorption is delaying pressure investigation because it provides an extra supply to gas production besides the free gas. On the log-log PTA diagnosis plot, this impact is illustrated by a parallel time shift of the flow regimes. For example, in the long term drawdown behavior of MTFHWs, gas desorption results in an apparent time shift in the early linear flow, the regime which might be the only one affecting gas production during the well life. Figure 33 illustrates gas desorption impact through a comparison between a drawdown behavior of MTFHW with gas desorption and without desorption.

The importance of gas desorption impact lies on the time when pressure interference between two adjacent transverse fractures. Interference occurrence will be delayed due to gas desorption, and this factor directly affects recovery efficiency design.
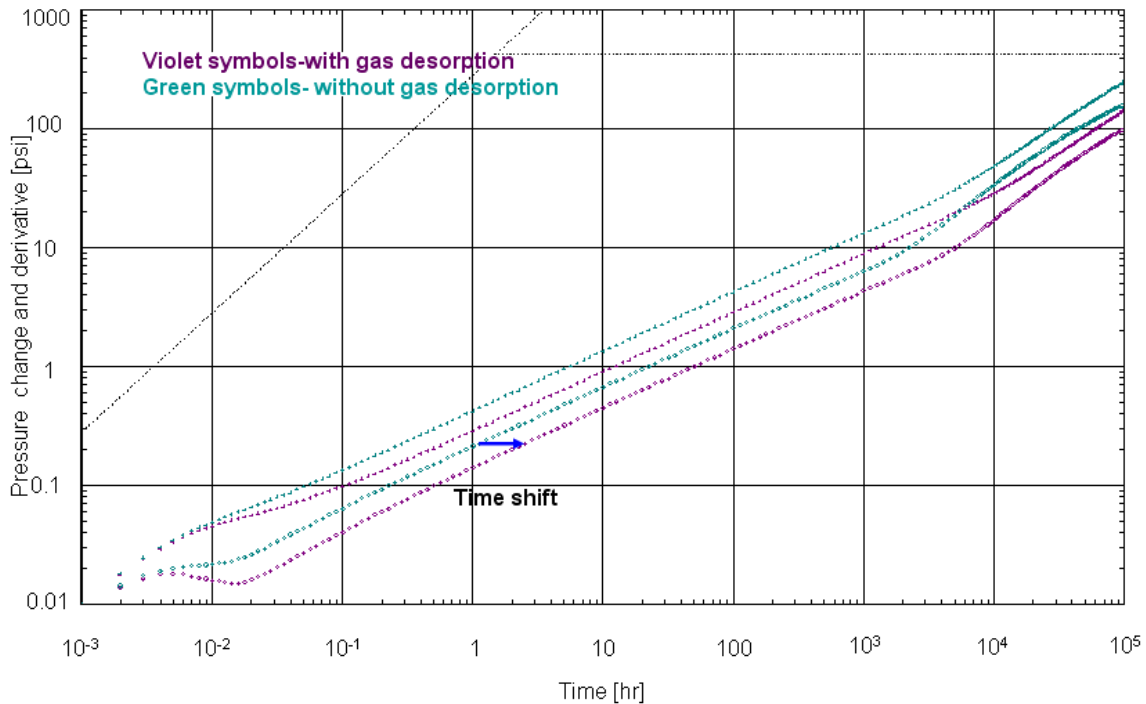
Figure 33. Gas Desorption Impact on Long Term Drawdown Behavior of MTFHWs

The time shift, which we can label the adsorption index, I_{ads} (define as the ratio of investigation time with gas desorption to that without gas desorption) depends on several parameters: ϕ, p_i, p_L and ρ_{ads}. To determine a correlation between time shift and those parameters, we did sensitivity studies to the parameters. Figure 34 shows the sensitivity study design.
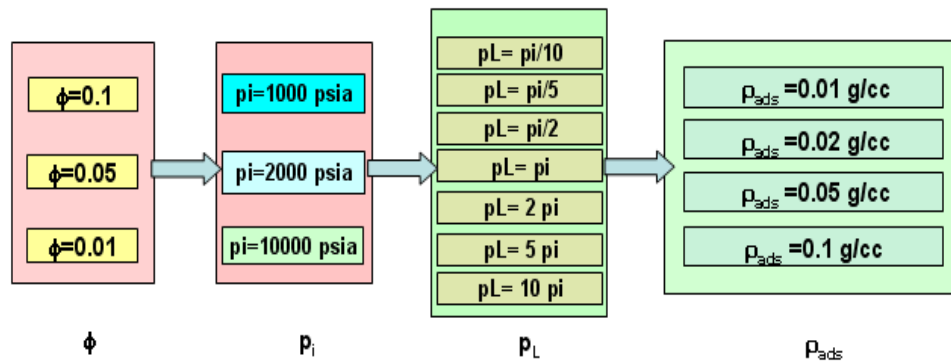
Figure 34. Time Shift (I_{ads}) Sensitivity Study

Figure 35 shows the sensitivity of the long term drawdown response to ρ_{ads} and Figure 36 shows that to p_L (symbols represent the case without gas desorption). Usually, ϕ and p_i are fixed, so we put Figures 35 and 36 to illustrate the sensitivity to ρ_{ads} and p_L. However, ϕ and p_i also impact the time shift, therefore actually, the sensitivity studies also include cases of various ϕ and p_i. The sensitivity studies give a correlation between I_{ads} and those four parameters and we made a program to calculate time shift.
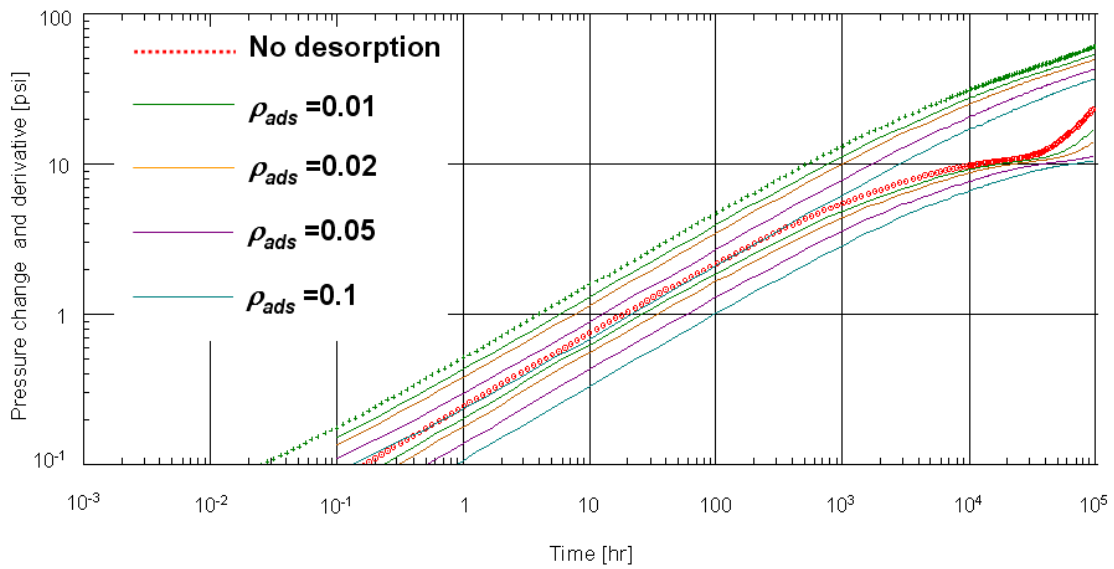
Figure 35. Illustration of Time Shift Sensitivity Study to ρ_{ads}
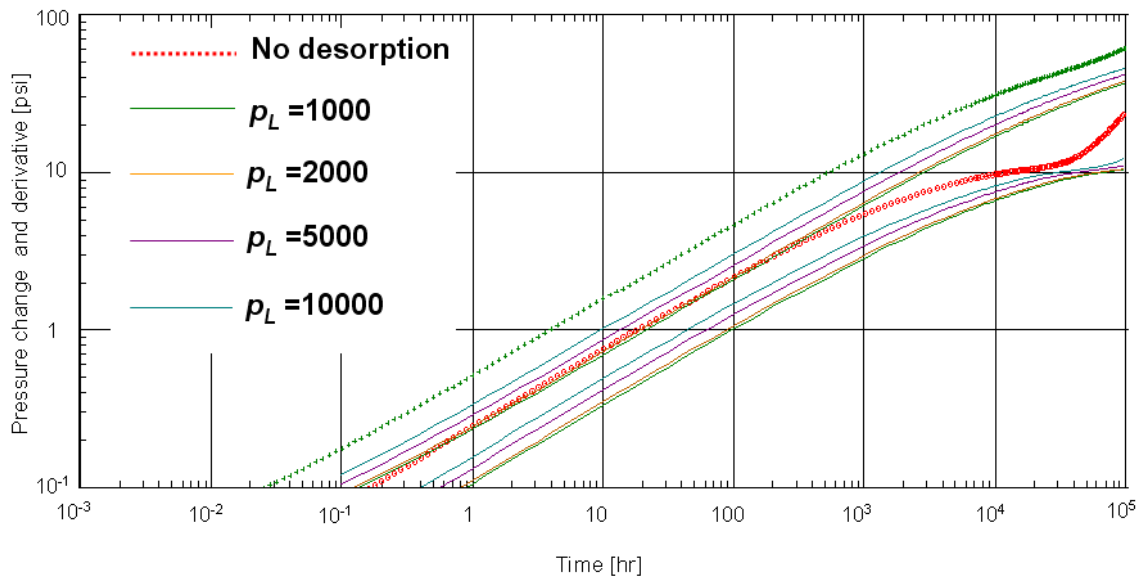
Figure 36. Illustration of Time Shift Sensitivity Study to p_L

We just use one case to illustrate how we extrapolate the relationship between time shift and the four-parameter combination.

Figure 37 shows the observed time shift versus ρ_{ads} for the case of ϕ=0.1 and

p_i=1000 psia. For various p_L, time shift appears as a linear function of ρ_{ads} with unit y-

intercept (Unit y-intercept is theoretical because 0 ρ_{ads} means no gas desorption, so the

time shift is 1, which means investigation time with desorption equals to that without

desorption). However the slope of the straight line depends on specific p_L, p_i and ϕ.
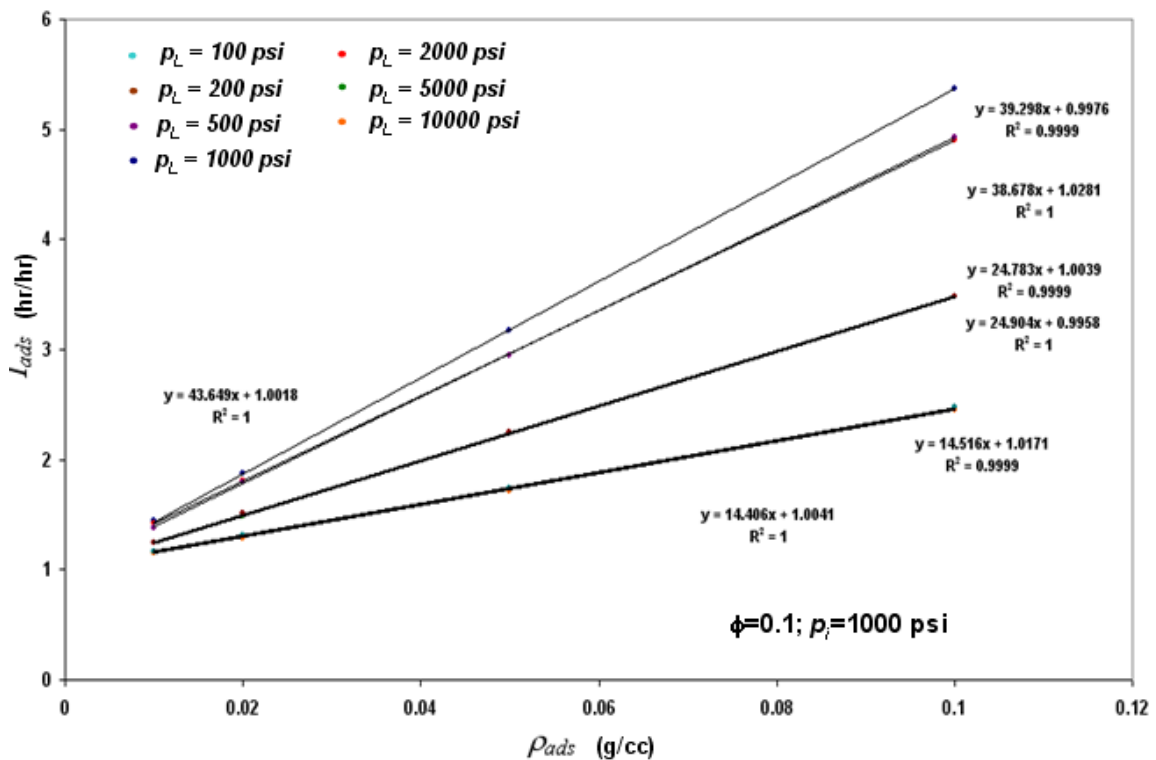
Figure 37. Illustration of Relationship between the Adsorption Index and ρ_{ads}

$$I_{ads} = t_{i,ads}/t_{i,noads} = slope \times \rho_{ads} +1 \dots\dots (11)$$

Where:

I_{ads} is the ratio of investigation time with desorption to that without desorption;

slope, the slope of the unit y-intercept linear function which correlates I_{ads} TS and ρ_{ads}.

Therefore, further we tried to correlate the slope of the linear function according to specific p_L, p_i and ϕ. Figure 38 shows the correlation.
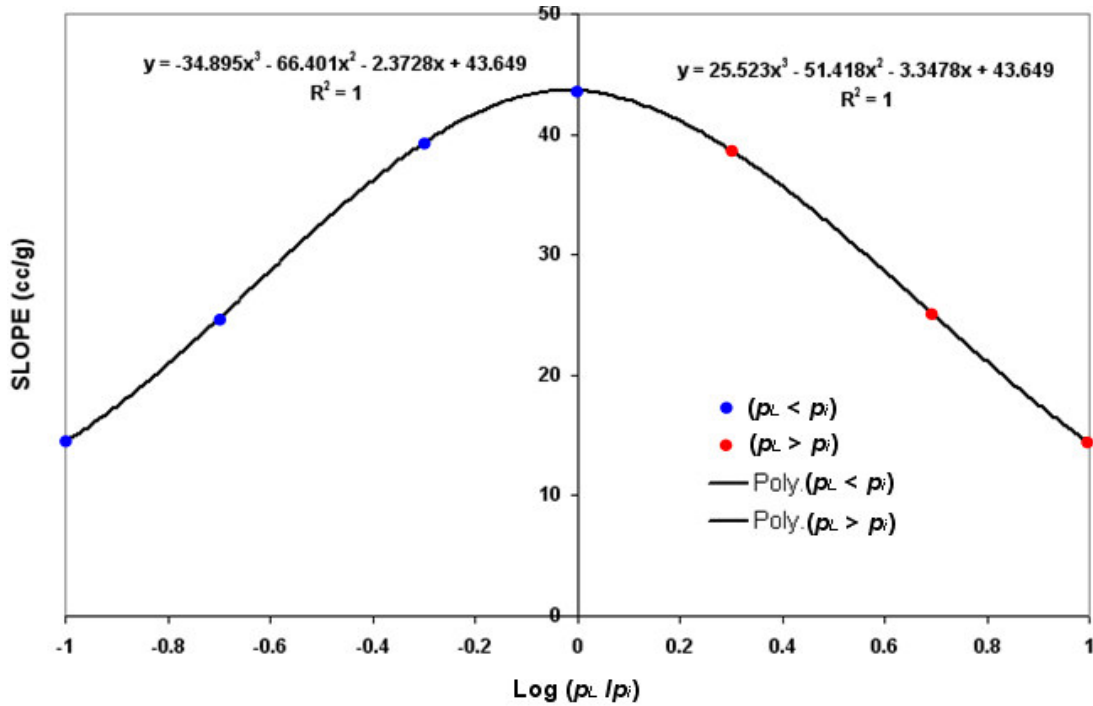
Figure 38. Illustration of Relationship between Slope and Logarithm of p_L over p_i

With a fixed ϕ, the slope is a cubic function of logarithm of p_L over p_i. However, this relationship is only applicable for the p_L with in the domain [$p_i/10$, $10p_i$]. Theoretically, the greater the ratio between p_L and p_i is, the smaller the slope will be. The cubic function is not decreasing as p_L increases or decreases. Therefore, the extrapolation is only effective when p_L is not very far from p_i. Additionally, the sensitivity studies are

run for some certain values of ϕ and p_i, but the correlation could be completed through

running more cases for other ϕ and p_i.

$$slope = c_1[\log(\frac{p_L}{p_i})]^3 + c_2[\log(\frac{p_L}{p_i})]^2 + c_3[\log(\frac{p_L}{p_i})] + c_4 \quad \dots\dots\dots\dots\dots\dots\dots\dots\dots (12)$$

Where:

c_1, c_2, c_3 and c_4 are the coefficients of the cubic function for the correlation between the

slope and logarithm of p_L over p_i.

Figure 39 shows the interface of the program. If we assign the specific ϕ, p_i, p_L

and ρ_{ads}, I_{ads} can be calculated. The logic can be divided into two steps: first, we use ϕ,

p_i and p_L to determine the so-called slope; second, determine the time shift with the

calculated slope according to specific ρ_{ads}.

This program has some limitation: ϕ, p_i and ρ_{ads} should be fixed at specific

values, and p_L should stay within the domain $[p_i/10, 10p_i]$. However, within its domain,

the program does provide an accurate estimate for I_{ads} that can be used for well design

purposes. A more general result may be possible with additional work.

Instruction					
This spreasheet is applied under some specific limits:					
1.Initial pressure should be one of 1000, 5000 and 10000 psia					
2. pL should be inside the domain [pi/10, 10pi]					
3. adsorption density should be within the domain [0.01, 0.1]					
4. real porosity should be one of 0.1, 0.05 and 0.01.					
input cells					
φ			Choose one from 0.1, 0.05 and 0.01		
pi, psia			Choose one from 1000,5000 and 10000		
pL psia			Choose one value within the domain [pi/10, 10pi]		
Rho_ad, g/cc			Choose one value within the domain [0.01, 0.1]		
result cells					
log(pL/pi)			**Calculate**		
slope					
Twd/Twod					

Figure 39. Interface of Program for Calculating Time Shift

4.6 Implications of the Early Linear Flow

The importance of early linear flow to MTFHWs is not only because it might be the only essential regime to the gas production, but also because during this flow regime, permeability and fracture half-length has a relationship from which either of them can be estimated when the other one were known. Furthermore, the end of early linear flow indicates the pressure interference between two adjacent transverse fractures, and this makes this flow regime important to recovery efficiency and well fracture design.

4.6.1 Relationship between Permeability and Fracture Half Length

During first linear flow before pressure interference occurs, the MTFHW actually performs like a single vertical well with a long fracture, whose length is the sum of all

the created fractures in the MTFHW. During this period, the equation for pressure change Δp versus time is:

$$\Delta p = m_{lf} \sqrt{\Delta t} + (\frac{\pi}{3})(\frac{m}{1.151})\frac{kx_f}{k_f w} \quad\text{...} \quad (13)$$

Where:

Δp, pressure change;

m_{lf}, the slope of a graph of pressure versus the square root of elapsed time;

Δt, elapsed time;

m, the slope of a graph of pressure versus log Δt;

k, formation permeability;

x_f, hydraulic fracture half length;

k_f, fracture permeability;

w, fracture width;

The equation for the pressure derivative is given by:

$$\Delta p^{'} = \frac{1}{2} m_{lf} \sqrt{\Delta t} \quad\text{...} \quad (14)$$

Where:

$\Delta p^{'}$, the derivative of pressure change with respect to the logarithm of elapsed time;

In turn, the product of $x_f k^{0.5}$ is related to m_{lf} by:

$$x_f \sqrt{k} = (\frac{4.064qB}{m_{lf} h})(\frac{\mu}{\phi c_t})^{1/2} \quad\text{...} \quad (15)$$

Where:

q , well flow rate;

B , the fluid formation volume factor;

h , the formation thickness;

μ , the fluid viscosity;

ϕ , the formation porosity;

c_t , the total compressibility;

Note: since the fluid is gas, the properties of gas including B, μ and c_t changes apparently as pressure changes, here we use the average values for these properties in order to take this consideration into account.

Therefore, the product of square root of time and fracture half-length is a constant. However for MTFHWs, the x_f is not fracture half length of only one transverse fracture but the summed half length of all the transverse fractures. This relationship is valuable because if we can estimate either of these two parameters if we know the other one: if summed fracture half-length can be determined told from microseismic measurement, reservoir permeability can be estimated; in contrast, if permeability is known, summed fracture half-length can also be estimated (Figure 40).
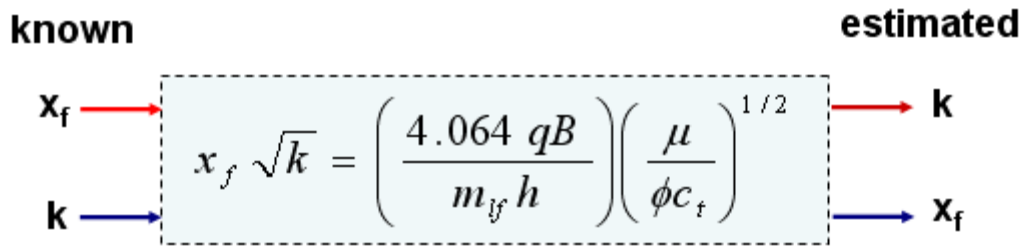
Figure 40. Application of the Relationship between k and x_f

4.6.2 Time of Fracture Interference

Ehlig-Economides (1992) provided an equation to estimate pressure investigation depth for linear flow.

$$x_i = 2\sqrt{\frac{kt}{948\phi\mu c_t}} \qquad (16)$$

Where:

x_i , the pressure investigation depth;

μ , the fluid viscosity;

ϕ , the formation porosity;

c_t , the total compressibility;

k , formation permeability;

t , elapse time;

Note: the fluid properties including B, μ and c_t here are the average values considering the fluid is gas because the properties of gas changes apparently as pressure changes.

The transform of Eq 14 will give Eq 15, by which we can estimate the pressure investigation time at some investigation depth.

$$t = \frac{948 \phi \mu c_t x_i^2}{4k} \dots\dots\dots\dots\dots\dots\dots\dots\dots\dots\dots\dots\dots\dots\dots\dots\dots\dots\dots\dots\dots\dots \text{(17)}$$

For MTFHWs, if we know the fracture spacing, we can estimate the time when pressure interference between two adjacent transverse fractures occurs. However, in shale gas reservoir, gas desorption impacts the pressure investigation. For the same pressure investigation depth, the corresponding investigation time with the existence of gas desorption will be larger than that without gas desorption. Therefore, the estimation of interference time should take gas desorption impact into account.

The estimate to interference time with the consideration of gas desorption can be done by combining the pressure investigation depth calculation and time shift calculation. If we know the permeability and fracture spacing, we can apply Eq 17 to calculate a time which doesn't take gas desorption into account. Then referring back to the program we made to calculate the time shift, we can calculate the time shift according to the specific ϕ, p_i, p_L and ρ_{ads}. The product of the time we calculated from Eq 17 and time shift calculated from the program can give a fracture interference time that which takes gas desorption into account.

4.6.3 Fracture Spacing Design for Interference at a Specific Time

The pressure investigation time calculation modified by the adsorption index affects the well design. If permeability is known, the well can be designed for fractures

to interfere at a specified time by spacing fractures accordingly. We can use an example

to illustrate this how to use I_{ads} to determine the fracture spacing.

Assume that a formation has the following properties: ϕ=0.1; p_i=5000 psia; p_L

=2500 psia; ρ_{ads} = 0.1 g/cc; k= 0.001 md at a given location, and that the well is to be

designed for fractures to interfere after 3.5 years. So first, according to the parameters ϕ,

p_i, p_L and ρ_{ads}, we calculate I_{ads} by the program at 2.38. Without gas desorption, the

corresponding interference time without desorption is 3.5 years /2.38 = 1.47 years. Then

we can use Eq 15 to calculate the pressure investigation depth after 1.47 years, and it is

200 ft. Therefore, we can design the fracture spacing at 400 ft, and we can say that a 400

ft fracture spacing will result in the fracture interference occurring after 3.5 years at this

reservoir location.

Chapter V will now illustrate the application of what has been learned from

sensitivity studies on actual field data from the New Albany shale gas wells.

CHAPTER V

FIELD CASE STUDY: NEW ALBANY SHALE

In this Chapter, Well A is used to illustrate the concepts that have been introduced in previous chapters. Both production and pressure transient data (one buildup) were collected as well as reservoir properties, fluid properties and well information. After processing the production/pressure data by unified BU-RNP method, we analyzed the data as a virtual constant rate pressure drawdown. Production analysis is also performed. We discuss the recovery facto issue based on the EUR estimation from the Valko (2009) approach. Also discussed is the special impact of gas desorption due to the low reservoir pressure in the case of Well A.

5.1 Field Data and Information Collection and Synthesizing

Production data for and one approximately 1 year, from Oct-03-2008 to Sep-13-2009, and one pressure buildup have been recorded for the Well A. The well completion diagram (Figure 41), fracturing job records, fluid properties, reservoir properties and gas desorption reports are also available. Table 6 lists the well, reservoir and fluid properties.

Gas adsorption data for a core sample from another well (Well B) is used for the analysis. It is assumed that these data are applicable for Well A because the 2 wells share almost the same reservoir conditions. Following is the calculation to determine ρ_{ads} from core analysis data:

$$\rho_{ads}$$
$$= 0.3048^3 \times \rho_{gas}^{surf} \times \rho_{rock} \times V_L$$
$$= 0.3048^3 \times 0.0008 g/cc \times 2.372 g/cc \times 125.8 scf/ton$$
$$= 0.00648 g/cc \qquad\qquad\qquad \text{.. (18)}$$

Table 7 synthesizes the gas adsorption information from core analysis with parameters to be loaded into Ecrin for analysis.

The estimation of fracture length of Well A is unavailable due to the lack of microseismic data. However, the microseismic data for Well B drilled in summer 2009 and its fracturing job record provide an estimation of the fracture length of that well. Table 8 shows the fracturing fluid injection amount for the first three stages and their corresponding fracture half-lengths. Assuming a correlation between the amounts of fracturing fluid (Nitrogen) and the fracture length, we estimated what may be the fracture lengths for Well A.

Nitrogen-fracturing efficiency, the ratio of fracture half-length to nitrogen volume used in fracturing job can be captured. Under the assumption that the nitrogen-fracturing efficiency is the same for Well A, the fracture half length of each stage of Well A can be estimated. Table 9 shows the estimation of half-fracture length for each stage of Well A. By applying the nitrogen-fracturing efficiency of Well B, 1.263 ft/Mscf, average fracture half length of Well A is estimated as approximately 1300 ft.
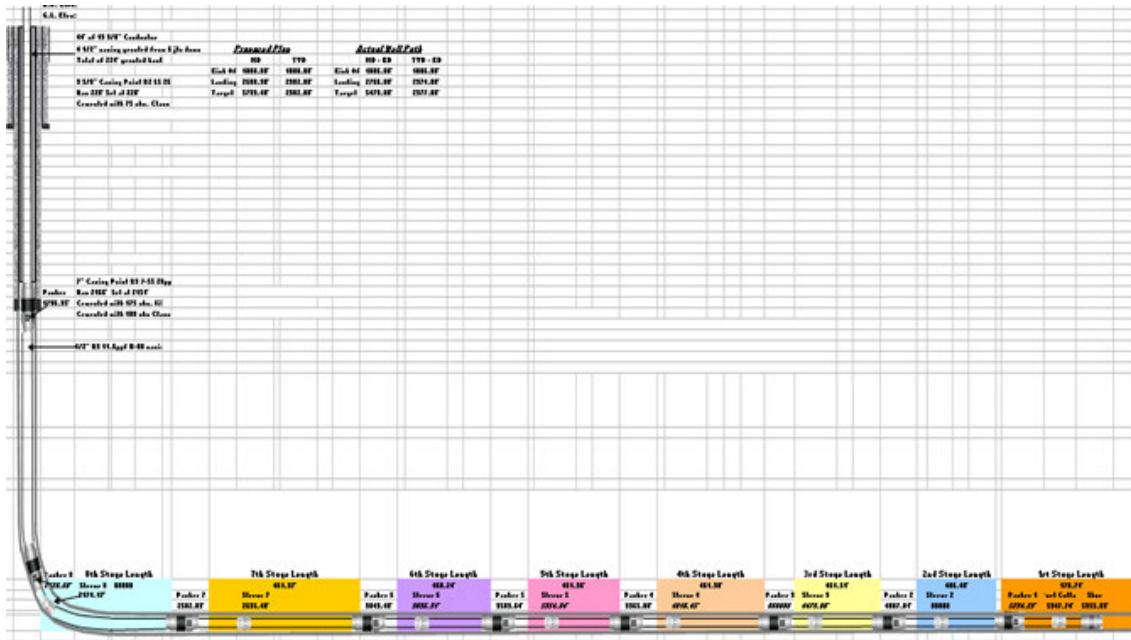
Figure 41.Well Structure of Well A

Table 6. Well, fluid and reservoir information of Well A

Well information	
well type	multi-transverse fractured horizontal well
number of well stage	8
L, well length, ft	3300
r, well radius, ft	0.375
fluid properties	
fluid type	gas
composition fraction	methane 84.39%; CO_2, 0.27%, N_2, 11.56%; other 3.78%
χ, specific gravity	0.626
reservoir information	
reservoir depth, ft	2382
T_r, reservoir temperature, ºF	89
P_i, reservoir pressure, psi	714
reservoir pressure gradient, psi/ft	0.3
ϕ, porosity	0.06
ρ_{rock}, rock density, g/cc	2.372

Table 7. Gas Adsorption Parameters for Well A

p_L, Langmuir pressure, psia	1044
V_L, Langmuir volume, scf/ton	125.82
V_L, Langmuir volume, cc/g	3.563
ρ_{rock}, rock density, g/cc	2.372
ρ_{ads}, adsorption density, g/cc	0.00648

Table 8. Fracture Half Length and Fracturing Used Nitrogen Volume Records

(Well B, Stage 1,2 and 3)			
Stage #	x_f, ft	total nitrogen in use, Mscf	ratio x_f/N_2
1	1190	1081	1.101
2	1650	1152	1.432
3	1260	1003	1.257
average nitrogen-fracturing efficiency			1.263

Table 9. Fracture Half Length Estimation for Well A

Stage #	total nitrogen in use, Mscf	x_f, ft
1	1004.1	1268
2	1001	1264
3	1001.4	1265
4	1002	1266
5	1002.5	1266
6	1002.5	1266
7	1002.8	1267
8	1003.3	1267
average nitrogen-fracturing efficiency	1.263	1266

5.2 Production/Pressure Data Processing by Unified BU-RNP Method

About one-year production rate and pressure data of Well A is recorded (Figure 42).There is one pressure build up which lasted 9 days but pressure data were only recorded once a day. The buildup is supposed to be used for pressure transient analysis. However, due to its sparse data frequency, the buildup doesn't give a very satisfying result.

Therefore, we use unified BU-RNP method to transfer this production process into a virtual constant rate pressure drawdown behavior for diagnosis. We selected the only build up in the production history as the data source of PTA processing, and also processed the whole PDA data by RNP. Figures 43 and 44 separately show the process of PTA processing and PDA processing, and the sub-steps are marked by arrows. Finally, we combined the results from PTA processing and that from PDA processing, and got a diagnostic plot of the virtual constant rate pressure drawdown behavior (Figure 45).
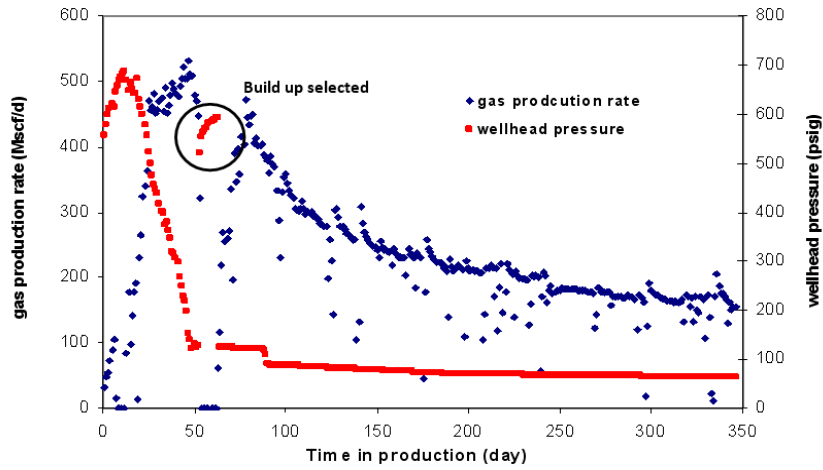
Figure 42. Production Rate and Pressure Data of Well A
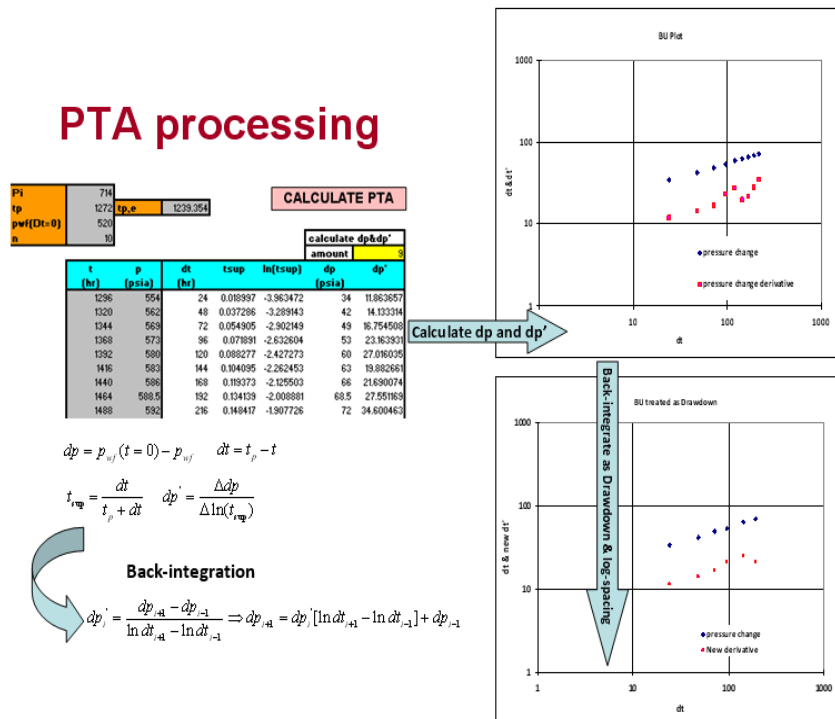
Figure 43. Unified BU-RNP Processing of PTA Data of Well A

PDA processing
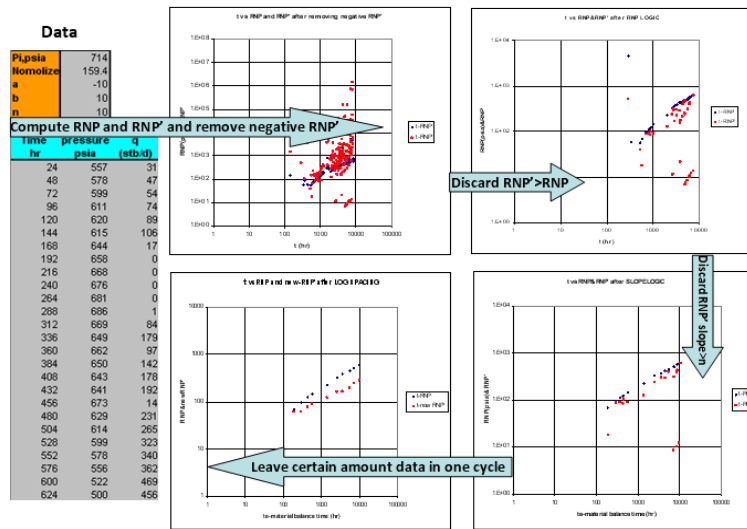
Figure 44. Unified BU-RNP Processing of PDA Data of Well A
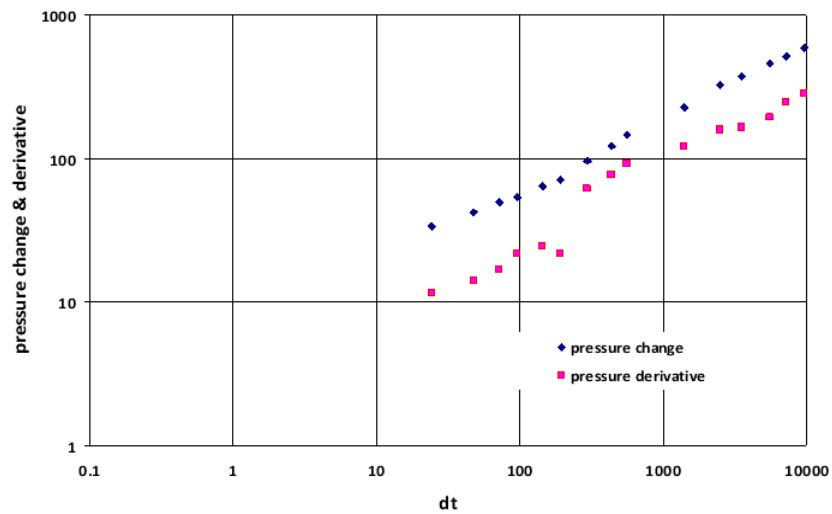
Figure 45. Unified BU-RNP Virtual Drawdown of Well A

5.3 PTA and Production Analyses

Unified BU-RNP processing provides a unified plot, from which we can analyze the well and reservoir characteristics. On the unified plot, we can see the pressure change and derivative show a half slope extending, more than two square cycles. Half slope derivative curve last more than 1 square cycle indicates the early linear flow normal to transverse fractures, and this is the only one flow regime observable on this unified plot.

After processing the production/pressure data into a virtual constant rate drawdown behavior, we also performed the PTA analysis using commercial software. By loading the virtual drawdown data into Kappa Ecrin Saphir, we tried to find an appropriate drawdown model to match the input data. Figure 46 shows a model match for the virtual drawdown behavior.
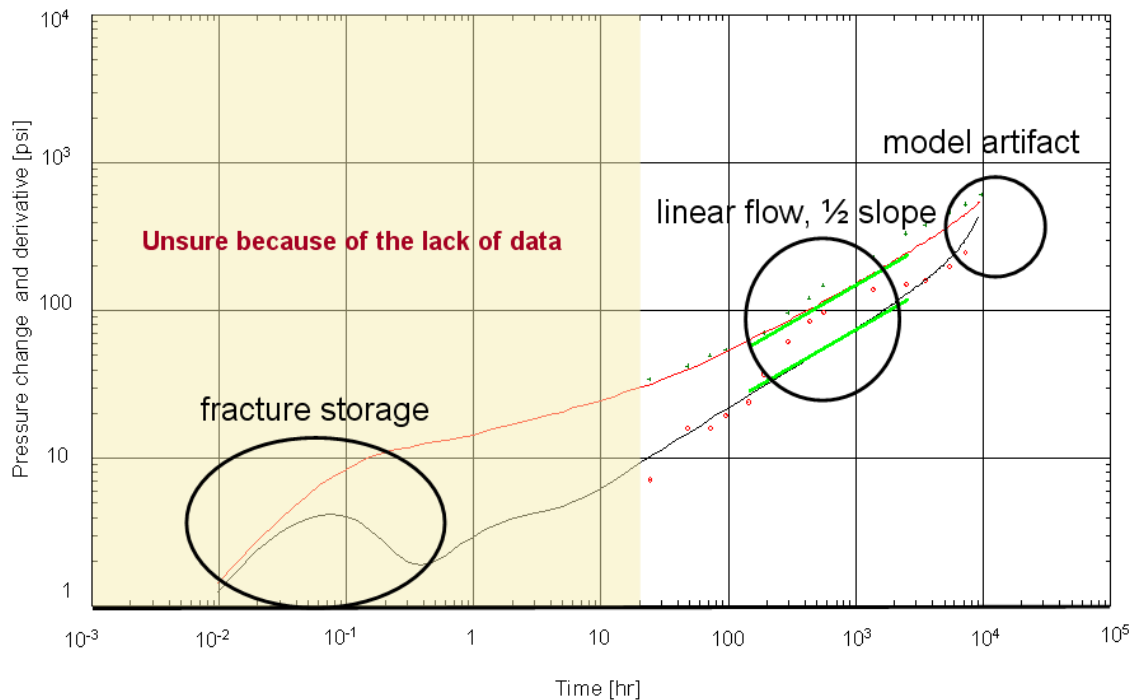
Figure 46. Virtual Drawdown Matching of Well A

The first data after unified BU-RNP processing is from 24th hour, so though the model provides fracture storage behavior, there is no match before 1 day due to the lack of early time buildup data. After that, as on the unified plot, we see the model pressure change and its derivative with half slope lasting about 2 square cycles. As discussed in Chapter V, this means the dominate flow geometry is linear flow normal to the fractures. The model shows an artifact at the end because constant rate drawdown exceeds the initial reservoir pressure. This model match gives the permeability of 0.000151 md and uses a fracture conductivity of infinite.

Production analysis is also performed to the production data of Well A by Kappa

Ecrin Topaze. Figure 47 shows the matching of production rate data and cumulative

production. Figure 48 is the rate normalized pressure (RNP) and its derivative plot.
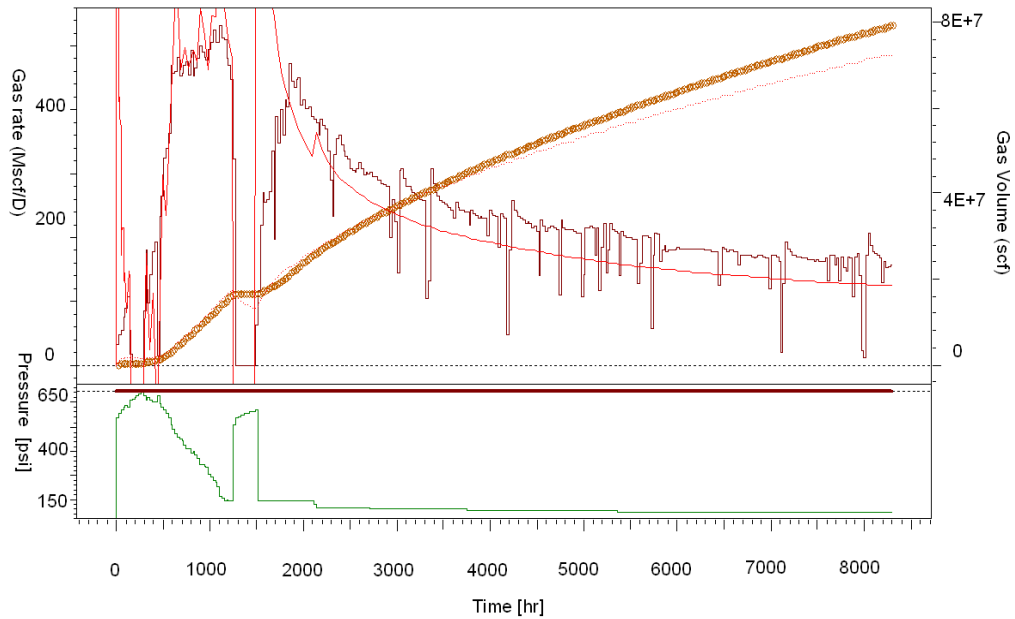
Figure 47. Rate and Cumulative Production Matching of Well A
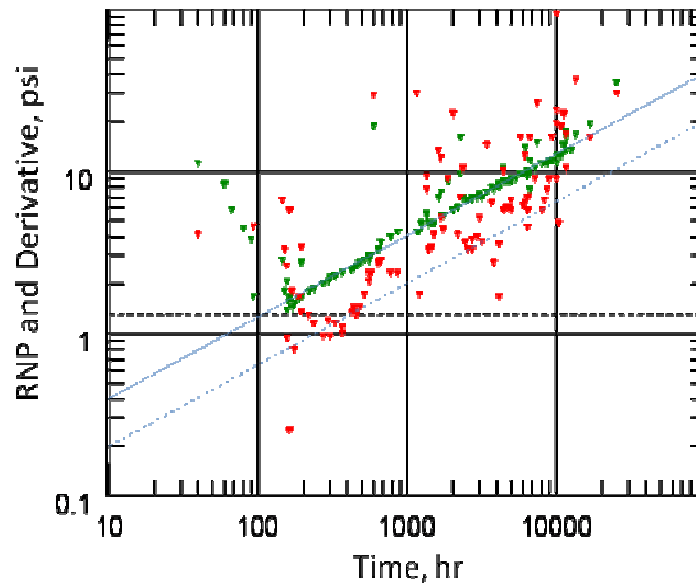
Figure 48. RNP and RNP Derivative Plot of Well A

Though the model we used in Topaze matching doesn't make the matching of production rate and cumulative production perfect as well, the RNP and RNP derivative plot does provide useful information about the flow regime. The half slope trend of RNP and its derivative lasts more than two square cycles, as before indicating that early linear flow normal to the transverse fractures is the dominant flow regime. Therefore we are confident to say that Well A just revealed the early linear flow and gas was only produced within a limited extent around transverse fractures, at least by the end time of the recorded production history.

The difficulty matching rate and cumulative production with Topaze is due to the inability of Topaze to properly model inherent limits in the production rate response to a step change in pressure. Kappa Engineering suggests adding skin in order to improve the

match, but in reality this does not work very well. It may be what is needed is a rate dependent skin that accounts for flow rate restriction by the wellbore itself.

Since we have an estimation to fracture half length of Well A, we can also apply the relationship between permeability and fracture half length to estimate the permeability. For Well A:

$$x_f \sqrt{k} = (\frac{4.064qB}{m_{lf}h})(\frac{\mu}{\phi c_t})^{1/2} = 128 \text{ ft-md}^{1/2} \dots\dots\dots\dots\dots\dots\dots\dots\dots\dots\dots\dots\dots\dots\dots\dots (19)$$

where m_{lf} =0.126 psi/cycle, from the plot of pressure versus square root of time, and the flow rate used for the RNP graph is the value of the last flow rate, q =156MSCF/d. If the summed fracture half length is 1300×8=10400 ft, permeability is 0.000151 md which almost agrees with the result from Saphir matching of the unified BU-RNP response.

Pressure investigation is also studied. The fracture spacing of Well A is about 400 ft. Therefore, during the early linear flow period, when pressure investigation depth reaches 200 ft, pressure interference will occur. Since we have estimated the permeability at 0.000151 md, we can estimate the time when pressure interference happens:

$$x_i = 2\sqrt{\frac{kt}{948\phi\mu c_t}} \Rightarrow t = \frac{948\phi\mu c_t x_i^2}{4k} = 1{,}760{,}906 \text{ hr} = 201.12 \text{ yr } (k=0.000151\text{md})\dots\dots(20)$$

This computation is conservative because it doesn't take gas desorption impact into account. Considering the specific reservoir properties, : ϕ=0.06; p_i=714 psia; p_L =1044 psia; ρ_{ads} = 0.00648 g/cc, we calculated the I_{ads} at 1.50. Therefore, if gas desorption is taken into account, the real time of interference should be 201.12 yr × 1.50= 301.68 yr.

That means in reality we can see the fracture interference after about 300 years. However, this well's life cannot be so long (surely much less than 100 years). For a given assumed time for the life of the well, the pressure investigation distance can be calculated. For example, after 100 years, the investigation distance is 115 ft.

5.4 EUR Estimation and Recovery Factor

We applied the Valko approach to estimate the EUR of Well A, and the result was calculated in Chapter III, in which the methodology was introduced. This approach indicated that the EUR of Well A is 132750 MSCF.

If we suppose the gas in place within the stimulated reservoir volume is the expected productive reserve, we can estimate the recovery factor by dividing EUR by the reserve in the SRV. The reserve in the SRV can be calculated through volume method, and both free gas and adsorbed gas should be considered.

Figure 49 shows the 2D map of SRV. We use volumetrics to calculate the gas in place within the SRV. Eq 21 shows how to calculate the gas in place within a certain shale gas reservoir volume.

$$GIP = GIP_{free} + GIP_{ads} = Ah\phi(1 - S_w)/B_g + Ah\rho_{rock}V_{ads} \quad\text{………………………………}(21)$$

Where:

GIP , gas in place

GIP_{free} , free gas in place

GIP_{ads} , adsorbed gas in place

A , drainage area

h, payzone thickness

ϕ, porosity

S_w, water saturation

B_g, gas volume factor

ρ_{rock}, rock density

V_{ads}, the gas volume can be adsorbed by a rock of unit mass;

Here, we calculated V_{ads} from Langmuir Isotherm.

$$V_{ads} = \frac{V_L p_i}{p_i + p_L} = \frac{125.8 \times 714}{714 + 1043.7} = 51.11 sfc/ton$$
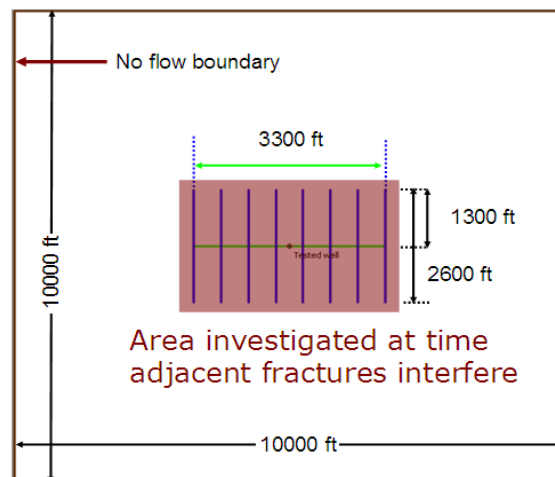
Figure 49. 2D Map of SRV of Well A

Table 10 shows the calculation of SRV geometry, free gas and adsorbed gas volume in SRV and recovery factor. The implied recovery factor for Well A is about 7.10%. This is very low for a gas reservoir. Two points can be mentioned. First, the

Valko extrapolation seems conservative. Referring back to Figure 14, the linear trend is more severely downward than the data, which actually seem to be leveling out. The Valko database may not have had very many MTFHWs, and there may be a need to extend the method for these wells. Second, the calculated interference time is far too great. Our analysis suggests that the fracture spacing in future New Albany shale wells should be smaller.

If conditions for another well are similar to those for Well A, using Eq 17, for a target interference time of 5 years, the spacing should be about 50 ft. The key point is that the fractures spaced closer together, the recovery factor will go up without changing the well response until the time of fracture interference. The fracture spacing should be a well design parameter. Either more fractures should be created, or for the same number of hydraulic fractures, the horizontal well length should be shorter.

Table 10. Recovery Factor Calculation of Well A

SRV geometry			
well length, ft	3300		
fracture half-length, ft	1300		
drainage length, ft	3300		
drainage width, ft	2600		
area, ft^2	$8.6{\times}10^6$		
pay zone thickness, ft	56		
drainage volume, ft^3	$4.8{\times}10^8$		
Free Gas		Adsorbed gas	
porosity	0.06	rock density, g/cc	2.372
water saturation	0.835	rock density, ton/cf	0.0672
gas in reservoir, rf	$4.76{\times}10^6$	mass of reservoir, ton	$3.23{\times}10^7$
gas volume factor, rf/scf	0.0217	storage capacity, scf/ton	51.11
gas in place, scf	$2.19{\times}10^8$	ad gas in place, scf	$1.65{\times}10^9$
gas in place, bscf	0.219	ad gas in place, bscf	1.649
Gas in place and recovery factor			
gas in place, bscf	$1.868{\times}10^9$		
Valko Reserve, bscf	0.1328		
Recovery Factor	7.10%		

5.5 Specialty of Low Reservoir Pressure and Comments on Well Design

The case of Well A is special because of its low initial reservoir pressure.
Generally, New Albany Shale is normally pressured and has a shallow reservoir depth of
only 2400ft. The low pressure gradient 0.3 psi/ft results in a abnormally low reservoir
pressure at 714 psi. This low reservoir pressure is a barrier for pursuing high gas
recovery. However, even with this low reservoir pressure, the EUR for an analogous
Well C is 99721 Mscf, which is more than the EUR for the vertical wells drilled in New
Albany Shale. This clearly justifies drilling additional MTFHWs might be a better
strategy to obtain more gas production.

For the well design, what really attracts our attention is the fracture interference time. We can design wells for fractures to interfere at a specified time by spacing the fractures accordingly. We can apply the time shift program to take gas desorption into account and use the pressure investigation depth formula to calculate a fracture spacing corresponding to the interference time we design. To pursue a higher recovery during a MTFHW's life, we recommend that the fracture spacing should not be too large. Specific strategies can be creating more transverse fractures if well length is fixed or shortening well length if the number of created fractures is fixed. The essence of the strategies actually is to increase fracture density, or rather to decrease fracture spacing. For Well A, since the well has been already completed, what can be done to increase the recovery is stimulating more fractures between each two adjacent fractures existing there.

CHAPTER VI

SUMMARY AND CONCLUSIONS

This chapter contains the summary of the contents in this thesis and conclusions according to the research work performed in this thesis.

6.1 Summary

This thesis is focusing on several aspects about shale gas. Based on the previous work and more detailed consideration, an appropriate conceptual model for shale gas is described. The "Triple porosity/ Dual permeability" model is considered as the reasonable model which describes the mechanisms of gas storage and transport in gas shale formations.

The Valko rate decline analysis approach was applied to estimate the EUR for 33 wells in New Albany Shale. Then we focused on long term drawdown pressure transient behavior in MTFHWs in shale gas reservoirs. We adopted the unified BU-RNP method to transfer the varying rate/varying pressure pressure/production data into a virtual constant rate pressure drawdown behavior, which can be matched against the existing constant rate pressure drawdown models. Drawdown model behavior is more straightforward than rate decline behavior for diagnosing well and reservoir characteristics because of the readily identified trends of characteristic slope of pressure change derivative. Sensitivity studies illustrated long term pressure drawdown behavior of MTFHWs in shale gas reservoirs, and typical flow regimes. From the early linear flow which is of great importance to MTFHWs, we concluded a relationship between

permeability and summed fracture half-length, and we also addressed the issue of time of pressure interference between two adjacent transverse fractures, which relates to recovery efficiency and a well design issue. Moreover, we also discussed that the main impact of gas desorption on long term drawdown behavior of MTFHWs is the delay of pressure interference, which is expressed as a time shift of the pressure change and its derivative curve.

We studied a field case, Well A in New Albany Shale. We synthesized the information about reservoir, well and fluid and recorded production/pressure data for about 1 year. The unified BU-RNP method was applied to process the data into a virtual constant rate drawdown behavior for long term pressure transient analysis. PTA and production analysis only indicated the early linear flow regime and model matching gave the permeability estimation as 1.51×10^{-4} md, which agrees with an estimation from the relationship for linear flow between permeability and fracture half length. The pressure investigation study indicated that the early linear flow take 200 years (conservative estimation without considering gas desorption), which is even much longer than the well's life to see the interfracture pressure interference. If gas desorption is taken into account, the time would be nearly 10 times longer making it even less likely ever to see the interference. EUR estimation helped calculate the recovery factor, and recovery factor reaches 7.10% if we consider the gas in place within SRV as productive reserve. To pursue higher recovery, we provided the recommendation of increasing fracture density or rather decreasing fracture spacing through creating more fractures or shorter well length. The special consideration of low reservoir pressure in Well A case is

considered as a disadvantageous factor to production recovery and performing long term well behavior analysis, but even with this low reservoir pressure, the higher EUR for Well A and its analogous wells compared to EUR for those vertical wells drilled in New Albany Shale offered great confidence of drilling additional MTFHWs.

6.2 Conclusions

Based on this study, the following conclusions can be drawn:

1. "Triple porosity/Dual permeability" Model is appropriate for describing gas storage and transport mechanisms in shale formations.

2. Long term pressure drawdown behavior of MTFHWs in shale gas reservoirs will encounter the following flow regimes in this order: fracture storage; early linear flow normal to the transverse fractures; interfracture pressure interference; compound linear flow; boundary flow.

3. During the early linearly flow period in MTFHWs, the system acts like a single fracture vertical well with the same total fracture length. The product of summed created fracture half-length and square root of permeability is a constant, so either of them can be estimated if the other were known.

4. In the shale gas reservoirs, the main impact of gas desorption is delaying pressure investigation, which is illustrated as a time shift of long term pressure drawdown behavior.

5. The time of interfracture pressure interference in MTFHWs is usually over hundred years because of the shale permeability in nanodarcy scale and the gas desorption

impact. So the pressure interference is hard to be seen even during the whole well life and early linear flow might be the only essential flow regime to MTFHW gas production.

6. Assuming an effective fracture half length for the transverse fractures, the formation permeability where Well A is located is about 1.51×10^{-4} md. By now the flow regime is still the linear flow normal to transverse fracture and it is unlikely to see pressure interference which will probably appear after nearly 200 years.

7. To pursue higher gas recovery of Well A, it is recommended to produce more transverse fractures or to shorten the horizontal well to reduce the fracture spacing.

8. The uncommonly low reservoir pressure in the Well A case might be a disadvantageous factor to production and long term well behavior analysis, however, even with such a low pressure, the EUR for analogous wells is about 10^5 MSCF that is much higher than EUR for vertical wells in the same play and encourages drilling additional MTFHWs.

6.3 Recommendations

We also made some recommendations for the future work based on our existing work. One idea would be to find a complete generalization for determination of the adsorption index for a continuous range of input parameters. Also, finding a way to determine permeability before the well design is finalized is quite important. If that were done, it would be really good to have microseismic on a well where permeability is known because this could help understand how good is the correlation between the

fracture length seen in microseismic and what is estimated from long term production. Moreover, to perform a better pressure transient analysis, we need pressure transient data with good quality, such as a pressure build ups with higher data frequency.

REFERENCES

Al-Kobaisi, M., Ozkan, E., Kazemi, H., and Ramirez, B. 2006. Pressure-Transient
Analysis of Horizontal Wells with Transverse, Finite-conductivity Fractures.
Paper PETSOC 2006-126 presented at the Petroleum Society's 7th Canadian
International Petroleum Conference (57th Annual Technical Meeting), Calgary,
Alberta, Canada, 13-15 June.

Cipolla, C.L., Lolon, E.P., Erdle, J.C., and Rubin. B. 2009. Reservoir Modeling in
Shale-Gas Reservoirs. Paper SPE 125530 presented at the 2009 SPE Eastern
Regional Meeting, Charleston, West Virginia, 23-25 September.

Clarkson, C.R., Jordan, C.L., Ilk, D., and Blasingame, T.A. 2009. Production Data
Analysis of Fractured and Horizontal CMB Wells. Paper SPE 125929 presented
at the 2009 SPE Eastern Regional Meeting, Charleston, West Virginia, 23-25
September.

Ehlig-Economides, C.A. 1992. Computation of Test Area of Investigation in Nonradial
Geometries. Paper SPE 25020 presented at the European Petroleum Conference,
Cannes, France, 16-18 November.

Ehlig-Economides, C.A., Martinez Barron, H., and Okunola, D. 2009. Unified PTA and
PDA Approach Enhances Well and Reservoir Characterization. Paper SPE
123042 presented at the 2009 SPE Latin American and Caribbean Petroleum
Engineering Conference, Cartagena, Colombia, 31 May-3 June.

Freeman, C.M., Moridis, G., Ilk, D., and Blasingame, T.A. 2009. A Numerical Study of

Performance for Tight Gas and Shale Gas Reservoir Systems. Paper SPE 124961 presented at the 2009 SPE Annual Technical Conference and Exhibition, New Orleans, Louisiana, 4-7 October.

Ilk, D., Rushing, J.A., Perego, A.D., and Blasingame, T.A. 2008. Exponential vs. Hyperbolic Decline in Tight Gas Sands-Understanding the Origin and Implications for Reserve Estimates Using Arps' Decline Curve. Paper SPE 116731 presented at the 2008 SPE Annual Technical Conference and Exhibition, Denver, Colorado, 21-24 September.

Arthur, J.D., Bohm, B., and Layne, M. 2008. Hydraulic Fracturing Considerations for Natural Gas Wells of the Marcellus Shale. Paper presented at the Ground Water Protection Council 2008 Annual Forum, Cincinnati, Ohio, 21-24 September.

Kalantari Dahaghi, A., and Mohaghegh. S.D. 2009. Economic Impact of Reservoir Properties, Horizontal Well Length Orientation on Production from Shale Formations: Application to New Albany Shale. Paper SPE 125893 presented at the 2009 SPE Eastern Regional Meeting, Charleston, West Virginia, 23-25 September.

Kuuskraa, V.A., Sedwick, K., and Yost II, A.B. 1985. Technically Recoverable Devonian Shale Gas in Ohio, West Virginia and Kentucky. Paper SPE 14503 presented at the SPE 1985 Eastern Regional Meeting, Morgantown, West Virginia, 6-8 November.

Lane, H.S., Lancaster, D.E., and Watson, A.T. 1990. Estimating Desorption

from Devonian Shale Well Test Data. Paper SPE 21272 presented at the SPE Eastern Regional Meeting, Columbus, Ohio, 31 October - 2 November.

Lane, H.S., Watson, A.T., and Lancaster, D.E. 1989. Identifying and Estimating Desorption from Devonian Shale Gas Production Data. Paper SPE 19794 presented at the 64th Annual Technical Conference and Exhibition of the Society of Petroleum Engineers, San Antonio, TX, 8-11 October.

Meyer, B.R., Bazan, L.W., Jacot, R.H., and Lattibeaudiere, M.G. 2010. Optimization of Multiple Transverse Hydraulic Fractures in Horizontal Wellbores. Paper SPE 131732 presented at the SPE Unconventional Gas Conference, Pittsburgh, Pennsylvania, 23-25 February.

Palacio, J.C., and Blasingame, T.A. 1993. Decline-curve Analysis Using Type Curves Analysis of Gas Well Production Data. Paper SPE 25909 presented as the SPE Joint Rocky Mountain Regional and Low Permeability Reservoir Symposium, Denver, Colorado, 26-28 April.

Rushing, J.A., Perego, A.D., and Blasingame, T.A. 2008. Applicability of the Arps Rate-Time Relationships for Evaluating Decline Behavior and Ultimate Gas Recovery of Coalbed Methane Wells. Paper SPE 114515 presented at the CIPC/SPE Gas Technology Symposium 2008 Joint Conference, Calgary, Alberta, Canada, 16-19 June.

Schepers, K.C., Gonzalez, R.J., Koperna, G.J., and Oudinot. A.Y. 2009. Reservoir

Modeling in Support of Shale Gas Exploration. Paper SPE 123057 presented at the 2009 SPE Latin American and Caribbean Petroleum Engineering Conference, Cartagena, Colombia, 31 May- 3 June.

Valko, P.P. 2009. Assigning Value to Stimulation in the Barnett Shale: A Simultaneous Analysis of 7000 Plus Production Histories and Well Completion Records. Paper SPE 119369 presented at the 2009 SPE Hydraulic Fracturing Technology Conference, Woodlands, Texas, 19-21 January.

van Kruysdijk, C.P.J.W, and Dullaert, G.M. 1989. A Boundary Element Solution of the Transient Pressure Response of Multiple Fractured Horizontal Wells. Paper presented at the 2nd European Conference on the Mathematics of Oil Recovery, Cambridge, England.

Wang, F.P., and Reed, R.M. 2009. Pore Networks and Fluid Flow in Gas Shales. Paper SPE 124253 presented at the 2009 SPE Annual Technical Conference and Exhibition, New Orleans, Louisiana, 4-7 October.

Wei, Y., and Economides, M.J. 2005. Transverse Hydraulic Fractures from a Horizontal Well. Paper SPE 94671 presented at the 2005 SPE Annual Technical Conference and Exhibition, Dallas, Texas, 9-12 October.

Zuber, M.D., Williamson. J.R., Hill. D.G., Sawyer, W.K., and Frantz. J.H. 2002. A Comprehensive Reservoir Evaluation of a Shale Reservoir-The New Albany Shale. Paper SPE 77469 presented at the 2002 SPE Annual Technical Conference and Exhibition, San Antonio, Texas, 29 September-2 October.

APPENDIX A

The appendix is going to reveal the specific gas desorption impact on shale gas well PTA behaviors. Also, it will explain why we use homogeneous reservoir model instead of dual porosity model in long term drawdown sensitivity study to MTFHWs and the study of New Albany Shale gas wells.

First, the conceptual model of shale gas reservoir is "Triple porosity/Dual permeability" Model. The valley on the derivative curve is a characterization of inter porosity flow, which happens in dual porosity reservoirs. We run the comparison test to illustrate the gas desorption impact on the both dual porosity characterization and pressure investigation. For convenience, we designed a simple constant rate drawdown behavior of a vertical well in shale gas reservoir (Table 11).

Table 11. Gas Desorption Impact Comparison Test Design

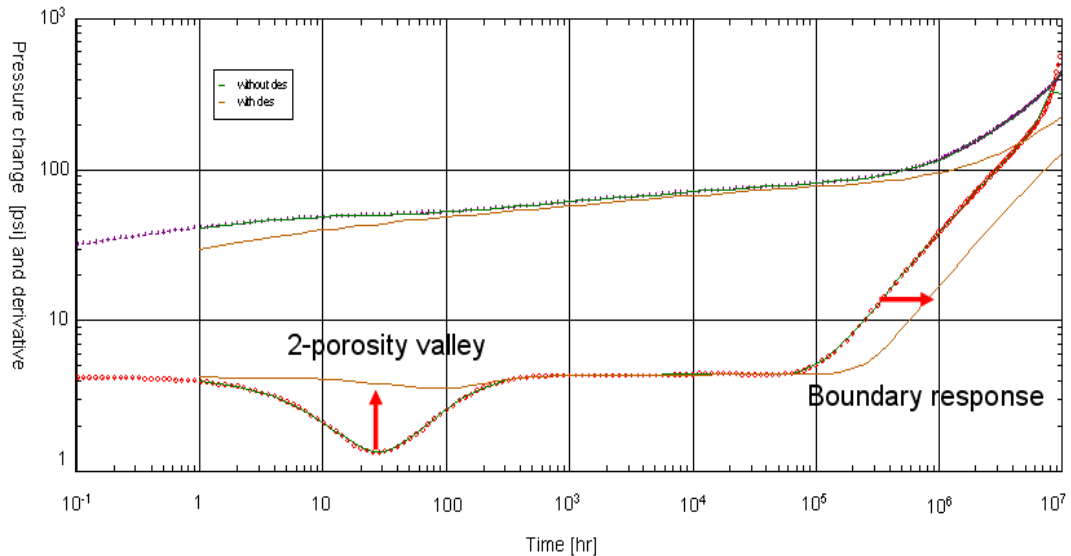|	without desorption	with desorption
well and fracture design		
well type	vertical	fractured vertical well
r, wellbore radius ,ft	0.3	0.3
reservoir properties		
h, ft	30	30
ϕ, porosity	0.1	0.1
P_i, initial reservoir pressure, psia	5000	5000
model design		
wellbore model	no wellbore storage	no wellbore storage
s, skin	0	0
reservoir model	two porosity	two porosity+ desorption
ω, storage ratio	0.1	0.1
λ, inter-porosity coefficient	1.00E-05	1.00E-05
k, permeability, md	0.1	0.1
p_L, psia	-	2000
ρ_{ads}, adsorption density, g/cc	-	0.1

Figure 50. PTA Behavior Comparison: With Desorption vs. Without Desorption

Figure 50 shows the comparison. Visually, besides delaying pressure investigation, gas desorption eliminates the intensity of interporosity flow, which is corresponded to the smaller valley on the derivative curve.

The reasons why we don't apply dual porosity model in the context include:

1. Dual porosity doesn't affect the long term drawdown behaviors, especially the formation of certain flow regimes;

2. Dual porosity valley might mask some characteristic PTA behavior;

3. If gas desorption impact is big enough, dual porosity characterization is likely to be eliminated, so PTA behavior is almost the same with the behavior with homogeneous reservoir model.

There are two characteristic parameters describing dual porosity reservoir:

$$\omega = \frac{(\phi C_t h)_f}{(\phi C_t h)_f + (\phi C_t h)_m} \approx \frac{V_{\phi f}}{V_{\phi f} + V_{\phi m}} \quad \text{.. (A-1)}$$

$$\lambda = \alpha \frac{k_m}{k_f} \quad \text{.. (A-2)}$$

Where:

ω, storage ratio, usually from 0.1 to 0.01;

λ, interporosity flow coefficient;

$V_{\phi f}$, the fracture space saturated by gas or volume of gas in fracture space;

$V_{\phi m}$, the pore space volume in matrix saturated by gas or the gas volume in matrix pores;

Take gas desorption into account, ω can be modified as:

$$\omega_{\text{mod}} = \frac{V_{\phi f} + S_{\phi f}\rho_{ra}}{V_{\phi f} + V_{\phi m} + S_{\phi f}\rho_{ra} + S_{\phi m}\rho_{ra}} \quad \text{.. (A-3)}$$

Where:

$S_{\phi f}$, the area of surface of fracture space exposed to matrix particles, ft^2;

$S_{\phi m}$, the area of surface of matrix pore space exposed to matrix particles, ft^2;

ρ_{ra}, Adsorbed gas volume released from unit exposed surface area, scf/ ft^2;

Because gas desorption reduces the intensity of interporosity flow:

$$\omega_{\text{mod}} = \frac{V_{\phi f} + S_{\phi f}\rho_{ra}}{V_{\phi f} + V_{\phi m} + S_{\phi f}\rho_{ra} + S_{\phi m}\rho_{ra}} > \frac{V_{\phi f}}{V_{\phi f} + V_{\phi m}} = \omega \quad \text{.......................... (A-4)}$$

$V_{\phi f}$, fracture space saturated by gas, cf

$V_{\phi m}$, the pore space volume in matrix saturated by gas, cf

This requires a precondition:

$$\frac{S_{\phi f}}{S_{\phi m}} < \frac{V_{\phi f}}{V_{\phi m}} \quad \ldots\ldots\ldots\ldots\ldots\ldots\ldots\ldots\ldots\ldots\ldots\ldots\ldots\ldots\ldots\ldots\ldots\ldots\ldots \quad \text{(A-5)}$$

Gas desorption is quantified by Langmuir model, and we want to reveal how the specific adsorption parameter, p_L and V_L affect the PTA drawdown behavior of shale gas wells.

First, we want to tell the relationship between V_{des} and ρ_{ra} and that between V_L and ρ_{ads}.

$$\rho_{ads} = \rho_{rock}\rho_{gas}^{surf}V_L \quad \ldots\ldots\ldots\ldots\ldots\ldots\ldots\ldots\ldots\ldots\ldots\ldots\ldots\ldots\ldots\ldots\ldots \quad \text{(A-6)}$$

$$V_{des} = V_{ph} - V_{pl} = \rho_{ra}S_{ex}^{surf} = \rho_{ra}(S_{\phi m} + S_{\phi f}) \quad \ldots\ldots\ldots\ldots\ldots\ldots\ldots\ldots\ldots\ldots\ldots \quad \text{(A-7)}$$

Where:

V_{des}, the total volume of desorbed gas;

V_{ph}, the adsorbed gas volume at the higher pressure;

V_{pl}, the adsorbed gas volume at the volume pressure;

S_{ex}^{surf}, the total area of exposed surface to matrix particles;

ρ_{ads} is nothing but another form of V_L, it transfers the adsorbed gas volume per unit rock mass into adsorbed gas mass per unit rock volume, so the essence is the same: the maximum amount of gas can be adsorbed.

ρ_{ra} is the V_{des} per unit exposed surface area, so they are positively correlated.

The tests include two series: $p_L<p_i$ and $p_L>p_i$. We perform the sensitivity study to ρ_{ads} and p_L to each series. Table 12 shows the basic test parameters, also we use a simple vertical well drawdown for convenience. Table 13 shows the sensitivity study design.

Table 12. Basic Design Settings-Gas Desorption Impact on Dual Porosity

Basic design settings - two porosity & gas desorption	
Well & Reservoir Geometry	
well type	vertical
length [ft]	10000
width [ft]	10000
reservoir boundary	no-flow
reservoir type	shale gas
reservoir and well parameters	
r, wellbore radius [ft]	0.3
h, pay zone [ft]	30
ϕ, porosity	0.1
PVT	
T_r, reservoir temperature [F deg]	212
P_i, initial reservoir pressure [psia]	2000
γ, specific gravity	0.7
Model settings	
wellbore model	No wellbore storage
s, skin	0
K, md	1
reservoir model	**two porosity + desorption**
ω, storage ratio	0.1
λ, interporosity coefficient	1.E-06

Table 13. Sensitivity Study Design

$p_L<p_i$ (2000)		$p_L>p_i$ (2000)	
p_L sensitivity, ρ_{ads}=0.1	ρ_{ads} sensitivity, p_L =1500	p_L sensitivity, ρ_{ads}=0.1	ρ_{ads} sensitivity, pL=2500
1500	10	2500	10
150	1	5000	1
15	0.1	10000	0.1
	0.01		0.01
	0.001		0.001
	0.0001		0.0001

Figures 51 to 54 separately show the sensitivity study results. Table 14 concludes the
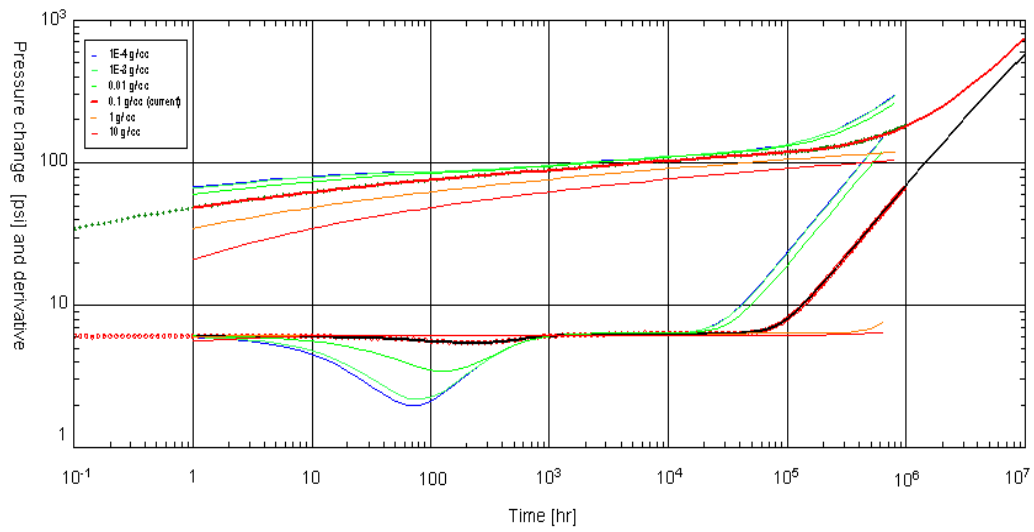
results.

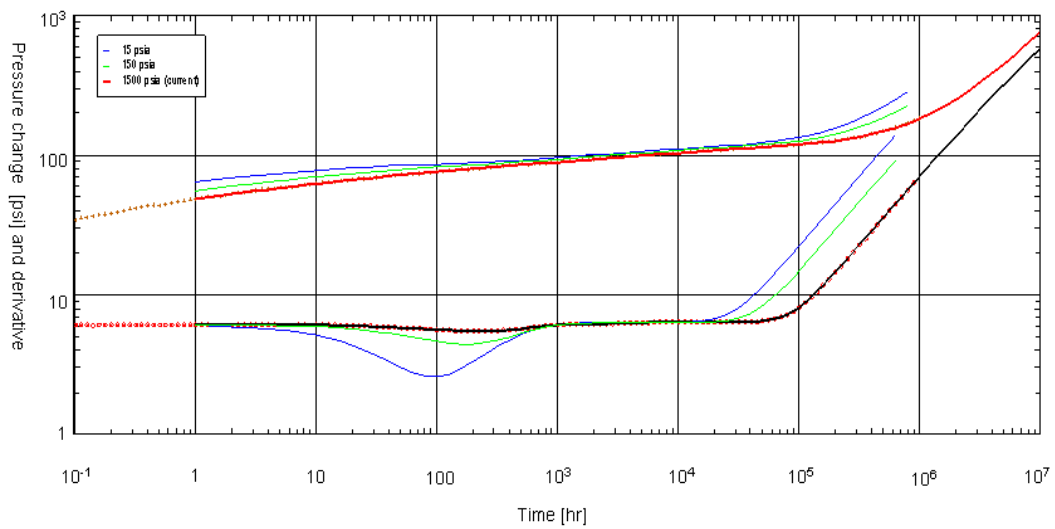Figure 51. Gas Adsorption Density Sensitivity Result - $p_L < p_i$

Figure 52. Langmuir Pressure Sensitivity Result - $p_L < p_i$

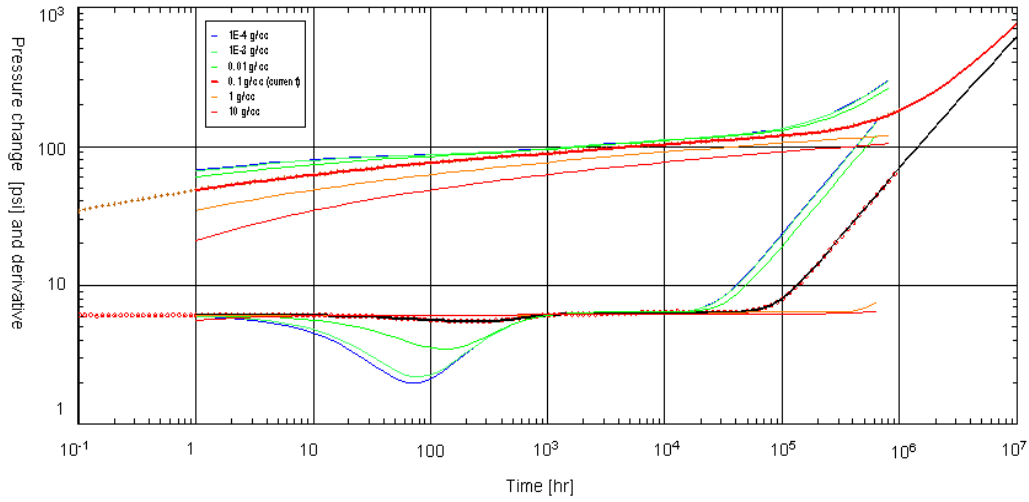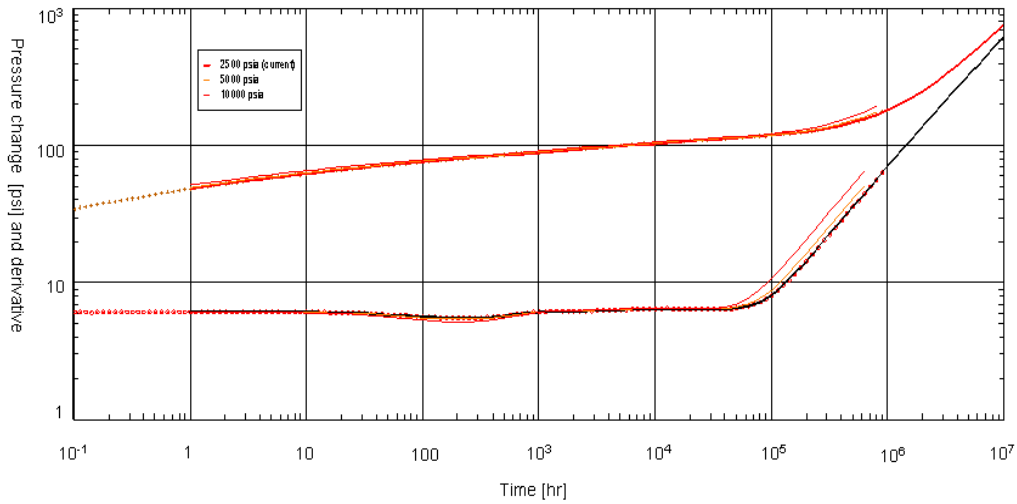Figure 53. Gas Adsorption Density Sensitivity Result - $p_L > p_i$

Figure 54. Langmuir Pressure Sensitivity Result - $p_L > p_i$

Table 14. Summary of Gas Desorption Impact on Shale Gas (Vertical) Wells

p_L vs. p_i	$\rho_{ads}\,(V_L)\downarrow$	$p_L \downarrow$
$p_L < p_i$	$\omega_{mod} \downarrow$, faster investigation	$\omega_{mod} \downarrow$, faster investigation
$p_L > p_i$	$\omega_{mod} \downarrow$, faster investigation	$\omega_{mod} \uparrow$, slower investigation

No matter which of $\rho_{ads}(V_L)$ or p_L changes, the decrement in ω_{mod} which indicates higher interporosity flow and results in a bigger derivative valley and the faster pressure investigation are essentially resulted from relatively smaller desorbed gas volume V_{des}.

For the impact on dual porosity characterization:

$$V_{des} \downarrow \Rightarrow \rho_{ra} \downarrow$$

Assume: $V_{\phi m} = aV_{\phi f}$ and $S_{\phi m} = bS_{\phi f}$, then

$$\frac{\partial \omega_{mod}}{\partial \rho_{ra}}$$

$$= \frac{S_{\phi f}[V_{\phi f}(1+a)+S_{\phi f}\rho_{ra}(1+b)]-(V_{\phi f}+S_{\phi f}\rho_{ra})S_{\phi f}(1+b)}{[V_{\phi f}(1+a)+S_{\phi f}\rho_{ra}(1+b)]^2}$$

$$= \frac{S_{\phi f}V_{\phi f}(1+a)+S_{\phi f}^2\rho_{ra}(1+b)-V_{\phi f}S_{\phi f}(1+b)-S_{\phi f}^2\rho_{ra}(1+b)}{[V_{\phi f}(1+a)+S_{\phi f}\rho_{ra}(1+b)]^2} \quad\dots\dots\dots\dots\dots\dots\text{ (A-8)}$$

$$= \frac{S_{\phi f}V_{\phi f}[1+a-(1+b)]}{[V_{\phi f}(1+a)+S_{\phi f}\rho_{ra}(1+b)]^2}$$

$$= \frac{S_{\phi f}V_{\phi f}[a-b]}{[V_{\phi f}(1+a)+S_{\phi f}\rho_{ra}(1+b)]^2}$$

According to Eq A-5 derived from the comparison test, $\dfrac{S_{\phi f}}{S_{\phi m}} < \dfrac{V_{\phi f}}{V_{\phi m}}$

recalling the assumption $V_{\phi m} = aV_{\phi f}$ and $S_{\phi m} = bS_{\phi f}$, this precondition equals to

$b < a$ or $a - b > 0$. Therefore:

$\dfrac{\partial \omega_{mod}}{\partial \rho_{ra}} > 0$. This indicates: $V_{des} \downarrow \xrightarrow{} \rho_{ra} \downarrow \xrightarrow{\frac{S_{\phi f}}{S_{\phi m}} < \frac{V_{\phi f}}{V_{\phi m}}} \omega_{mod} \downarrow$

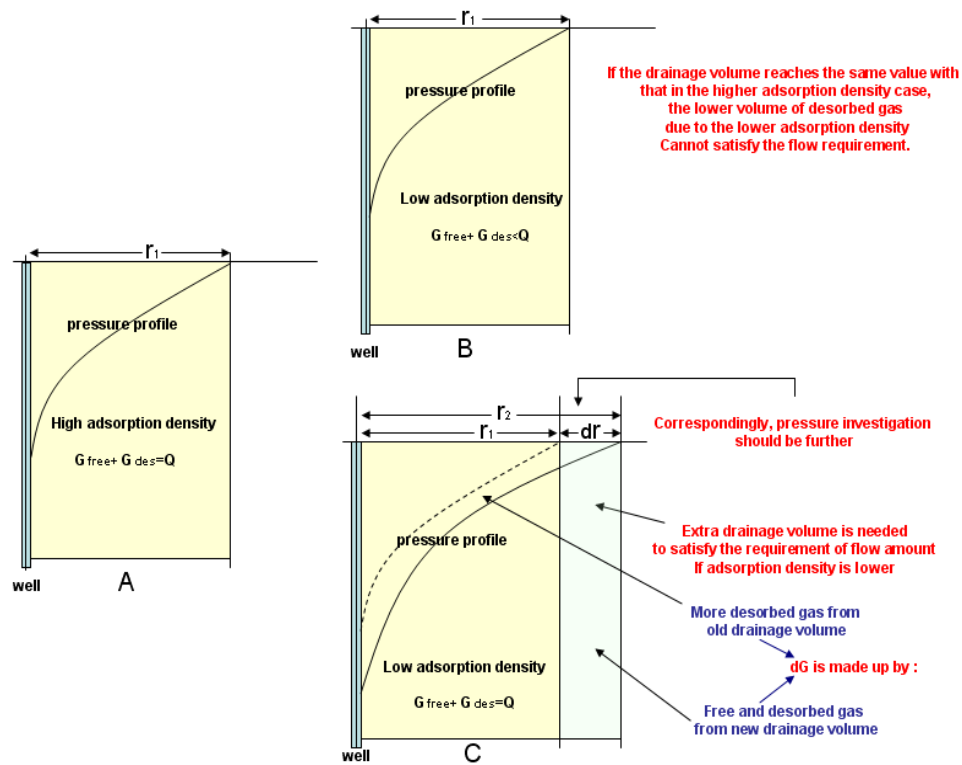For faster pressure investigation, Figure 55 shows the logic:

Figure 55. Faster Pressure Investigation Caused by Smaller Gas Desorption

Back to the smaller desorbed gas volume, Langmuir Isotherm comparison provides the logic for the four sensitivity studies. Figure 56 shows the smaller desorbed gas volume resulted from ρ_{ads} (or V_L) and p_L changes.
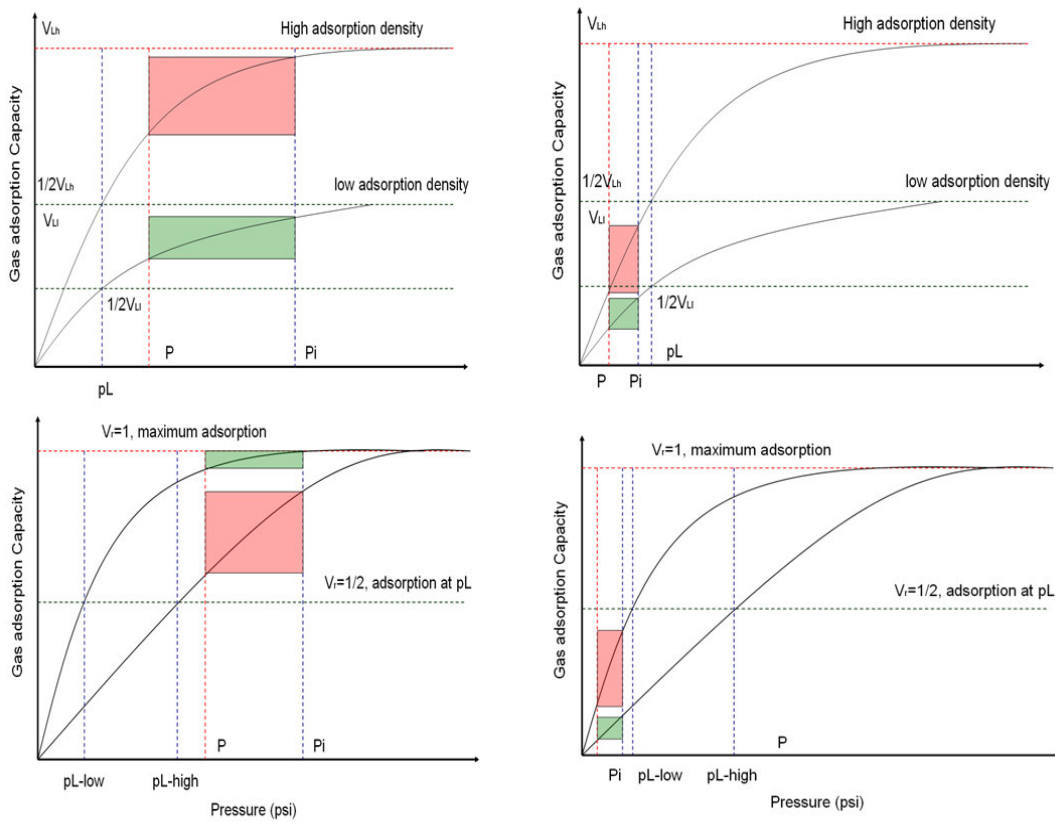
Figure 56. The Smaller Desorbed Gas Volume due to ρ_{ads} (or V_L) and p_L Changes

The logic is no matter $p_L<p_i$ or $p_L<p_i$, if p_L is the same, the lower ρ_{ads} (or V_L) isotherm gives smaller desorbed gas volume; when $p_L<p_i$, if ρ_{ads} (or V_L) is the same, the lower p_L isotherm gives smaller desorbed gas volume; when $p_L>p_i$, if ρ_{ads} (or V_L) is the same, the higher p_L isotherm gives smaller desorbed gas volume.

The Analytical derivation of this logic is shown below:

At initial pressure: $V_{p_i} = \dfrac{V_L p_i}{p_L + p_i}$

After pressure drops, at some certain pressure: $V_p = \dfrac{V_L p}{p_L + p}$;

So the gas desorption volume is:

$$V_{des} = V_{p_i} - V_p = \frac{V_L p_i}{p_L + p_i} - \frac{V_L p}{p_L + p} = \frac{V_L p_i (p_L + p) - V_L p (p_L + p_i)}{(p_L + p_i)(p_L + p)}$$

$$= \frac{V_L p_i p_L + V_L p_i p - V_L p p_L - V_L p p_i}{(p_L + p_i)(p_L + p)} = \frac{V_L p_L (p_i - p)}{(p_L + p_i)(p_L + p)} \qquad\qquad \text{…………………….. (A-9)}$$

For ρ_{ads} (or V_L):

$$\frac{\partial V_{des}}{\partial V_L} = \frac{\partial}{\partial V_L} \frac{V_L p_L (p_i - p)}{(p_L + p_i)(p_L + p)} = \frac{p_L (p_i - p)}{(p_L + p_i)(p_L + p)} \qquad\qquad \text{………………………..……...…… (A-10)}$$

Since all parameters are positive and $p < p_i$, so $\dfrac{\partial V_{des}}{\partial V_L} > 0$. Here we find that no matter

$p_L < p_i$ or $p_i < p_L$, and no matter what p is ($p > p_L$ or $p < p_L$), $\dfrac{\partial V_{des}}{\partial V_L}$ is always positive

We can conclude this as following: the lower ρ_{ads} (or V_L) is, the smaller V_{des} will be.

For p_L :

$$\frac{\partial V_{des}}{\partial p_L} = \frac{\partial}{\partial p_L} \frac{V_L p_L (p_i - p)}{(p_L + p_i)(p_L + p)}$$

$$= \frac{\dfrac{\partial [V_L p_L (p_i - p)]}{\partial p_L} \times (p_L + p_i)(p_L + p) - \dfrac{\partial [(p_L + p_i)(p_L + p)]}{\partial p_L} \times V_L p_L (p_i - p)}{[(p_L + p_i)(p_L + p)]^2}$$

$$= \frac{V_L (p_i - p)[p_L^2 + p_L (p + p_i) + p_i p] - V_L (p_i - p)[2 p_L + (p + p_i)]}{[p_L^2 + p_L (p + p_i) + p_i p]^2} =$$

$$= \frac{V_L p_L^2 (p_i - p) + V_L p_L (p_i - p)(p + p_i) + V_L p_i p (p_i - p)}{[p_L^2 + p_L (p + p_i) + p_i p]^2} \qquad\qquad \text{…………….. (A-11)}$$

$$- \frac{2 V_L p_L (p_i - p) + V_L p_L (p_i - p)(p + p_i)}{[p_L^2 + p_L (p + p_i) + p_i p]^2}$$

$$= \frac{V_L p_i p (p_i - p) - V_L p_L^2 (p_i - p)}{[p_L^2 + p_L (p + p_i) + p_i p]^2}$$

$$= \frac{V_L (p_i - p)[p_i p - p_L^2]}{[p_L^2 + p_L (p + p_i) + p_i p]^2}$$

If $p_i > p_L$, we should consider p further:

If $(p_i >)p \geq p_L$, then $p_i p - p_L{}^2 > 0 \Rightarrow \dfrac{\partial V_{des}}{\partial p_L} > 0 \Rightarrow p_L \downarrow, V_{des} \downarrow$;

If $p < p_L < p_i$, then $p_i p - p_L{}^2$ is not determinable. (if $p > p_L^2/p_i$, the result is applicable.)

If $pi \leq p_L$, there is only $p < p_i < p_L$, and this will result in:

$$p_i p - p_L{}^2 < 0 \Rightarrow \dfrac{\partial V_{des}}{\partial p_L} < 0 \Rightarrow p_L \uparrow, V_{des} \downarrow.$$

Therefore, we can conclude a flow chart illustrating the logic of gas desorption impact on shale gas well drawdown behavior (Figure 57).
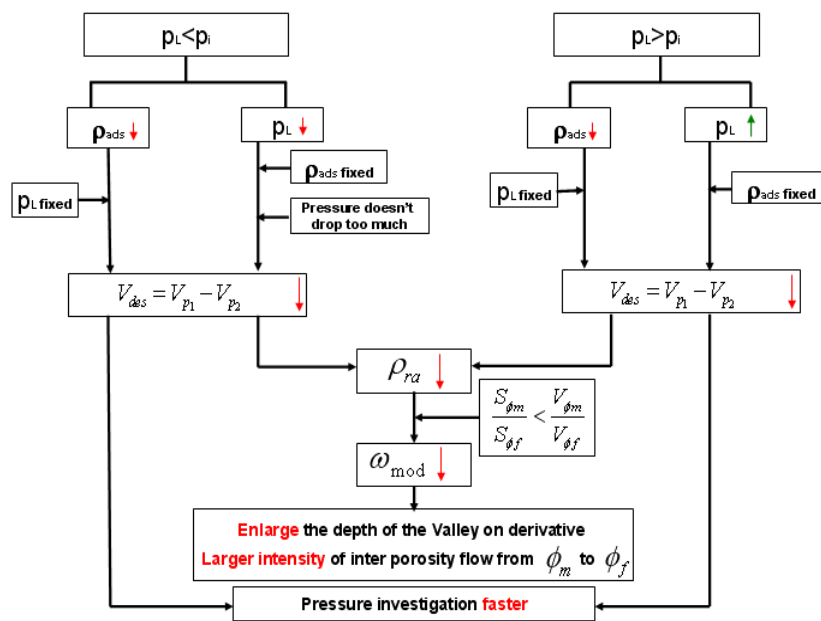

Figure 57. Gas Desorption Impact on PTA Behavior of Shale Gas Wells

VITA

Name: Bo Song

Address: 3116 TAMU - 719 Richardson Building
                   College Station, TX 77843-3116

Email Address: bo.song@pe.tamu.edu

Education: B.A., Petroleum Engineering, China University of Geosciences
                   (Beijing), 2008